

**Measurement of
lepton beam polarisation
at HERA**

Osamu Ota

High Energy Physics Group
Department of Physics
Tokyo Metropolitan University

February 10, 2005

Abstract

At HERA (Hadron Electron Ring Accelerator), which is built at DESY (Deutches Electron Synchrotron) laboratory in Hamburg, Germany, *ep* collider experiments have been carried out. During the long shutdown from 2000 to 2002, the luminosity of HERA has been increased by a factor of five and a longitudinally polarised lepton beam was provided for H1 and ZEUS experiments. With the longitudinally polarised lepton beam, it is expected that the Electro-Weak(EW) theory can be checked precisely. For these precise measurements, it is required that the precision of the measurement of lepton beam polarisation must be achieved within 2 %.

Polarisation has been measured with two independent detectors at HERA, the Longitudinal Polarimeter(LPOL) and the Transverse Polarimeter(TPOL). So far, the polarisation ratio of two values, LPOL/TPOL has been off by 10% from 1. In order to reduce this discrepancy, an alternative analysis method has been developed and checked. All polarisation runs, from October 2003 to August 2004, were analysed with this new method and the polarisation value was determined, and also the total systematic error was estimated.

Contents

1	Introduction	3
2	The Transverse Polarimeter	10
2.1	The Transverse Polarimeter	10
2.2	The Calorimeter	12
2.3	The Silicon Detector	17
2.3.1	The Silicon Detector	17
2.3.2	Clustering Algorithm	20
2.4	The Fibre Detector	20
2.5	The η - y transformation	22
2.6	The procedure of deriving the η - y curve	23
3	Polarisation Measurement	28
3.1	Polarisation at HERA	28
3.2	Compton scattering	29
3.3	Measurement of Transverse Polarisation	33
3.4	Measurement of Longitudinal Polarisation	36
4	The Fitting Method	37
4.1	The Fitting Procedure	37
4.2	The Fitting Parameters	39
4.3	Background Subtraction	41
4.4	Determination of parameter set	41
4.4.1	Stability against η range	41
4.4.2	Determination of the fitting range	42
4.4.3	Comparison between Data and Fit	47

5	Systematic Errors	51
5.1	Overview	51
5.2	Distance from the IP to the calorimeter	51
5.3	Vertical beam offset	52
5.4	Choice of the η - y curve	52
5.5	Change of the fitting range	52
5.6	Calibration of the calorimeter	54
5.7	Energy resolution of the calorimeter	54
5.8	Summary of systematic checks	56
6	Results and Discussion	57
6.1	Comparison with the LPOL	57
6.2	Focus Correction	59
6.3	Vertical beam offset	63
6.4	Comparison between two Polarisation \sim laser-left and laser-right \sim	67
6.5	The energy resolution	80
6.6	The calibration of the calorimeter	80
7	Conclusion	87

Chapter 1

Introduction

A simple question has been most interesting things for human being, that is, what is constituents of material? To clear up the question, scattering experiments have been done.

In 1911, Rutherford discovered a nucleus in the atom by using alpha particles as a probe. Probes with its wavelength shorter were used, in other words, with its energy higher, smaller component of the material could be seen. Today, structures of proton can be investigated by a high energy accelerator and believed that the world is made from quarks and leptons [1] and those are called elementary particles.

Theoretically, four fundamental forces are believed to exist, electromagnetic, weak, strong and gravity. Among them, the electromagnetic and the weak forces were unified by Glashow, Salam and Weinberg [2] and known as the Electro-Weak (EW) theory.

To increase probe's energy, colliding two beams is most efficient. HERA, the world's first unique ep collider, has been built at DESY and has been used to study the proton structure in deep inelastic scattering (DIS). In Figure 1.1 and 1.2 a schematic layout of the HERA ring and a drawing of that are displayed. Also, some parameters of the accelerator is shown in Table 1.1. In the HERA ring, a lepton beam (electron or positron) is accelerated, and the energy of the lepton beam can reach to 27.5 GeV, on the other hand the energy of proton beam reaches to 920 GeV. Therefore, the centre of mass is around 314GeV. 220 bunches of electron and proton are stored in each ring as a upper limit and two beams collide in every 96ns time interval. These beams have been provided to three experiments, ZEUS, H1 and HERMES. With ZEUS and H1, collider experiments have been done and

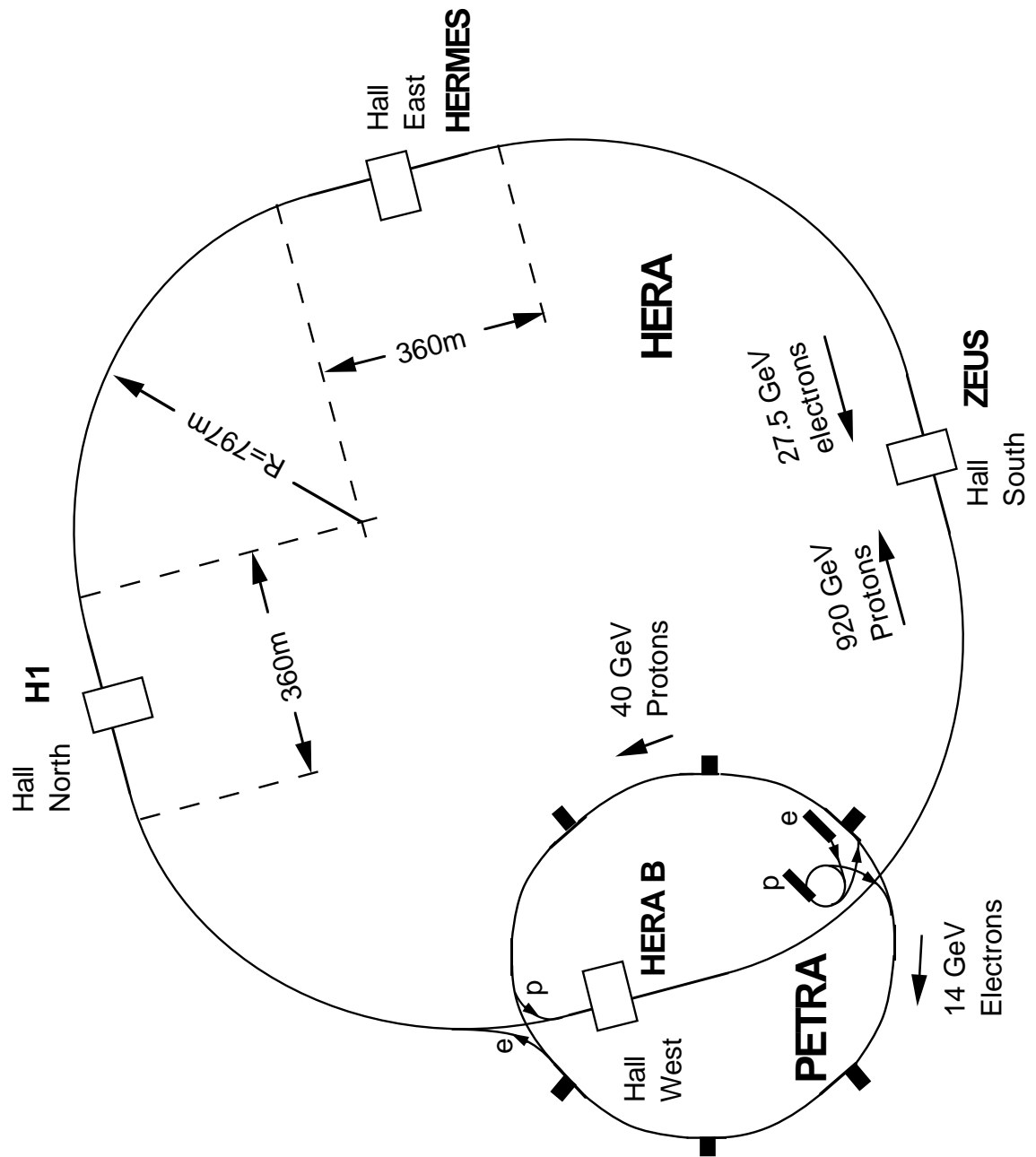


Figure 1.1: Schematic layout of HERA.

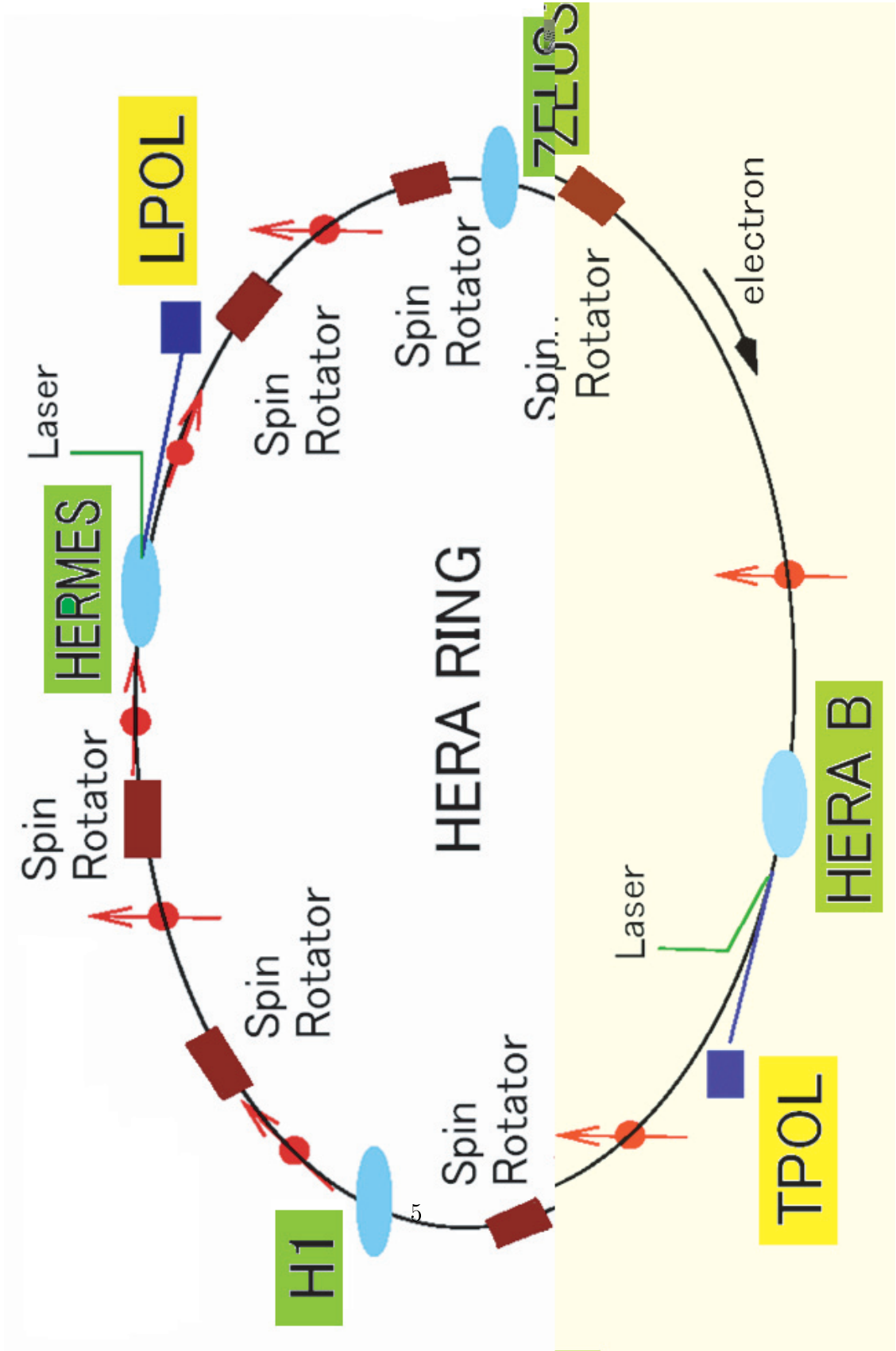


Figure 1.2: HERA ring.

HERA Beam	Electron	Proton
Circumference	6336 m	
Nominal Energy	30 GeV	820 GeV
Centre-of -mass Energy	314 GeV	
Luminosity per Interaction Point	$1.5 \times 10^{31} \text{ cm}^{-2}\text{s}^{-1}$	
Particle Current	60 mA	160 mA
Particle per Bunches	3.5×10^{10}	10^{11}
Number of Bunch Buckets	220	220
Maximum Number of Bunches	210	210
Beam Crossing Angle	Head-on Collision (0 mrad)	
Bunch Distance	28.8 m (96 ns)	
Beam Length at Max. Energy (1σ)	7.8 mm	110-150 mm
Beam Width at Interaction Point	0.3 mm	0.04 mm
Beam Hight at Interaction Point	0.04 mm	0.1 mm
Polarisation Time at 30 GeV	27 min.	-
Filling Time	15 min.	20 min.

Table 1.1: HERA design parameters [3]

with HERMES a fixed target experiment has done. During a long shutdown from 2000 to 2002, the HERA ring were improved in two points. One was the luminosity upgrade, another was that special magnet, called “spin rotator” were installed near the ep interaction regions at ZEUS and H1. For that improvements, a luminosity has increased five times higher than before and also it has been possible to use longitudinally polarised lepton beams. The reason of upgrades are confirmation of the EW theory precisely.

For example, at ZEUS and H1, the Charged Current (CC) cross section and the Neutral Current cross section have been measured as functions of the lepton beam polarisation. In Figure 1.3 and Figure 1.4, the CC cross section and the NC cross section measured and expected by MC are displayed. These pictures show that precise polarisation measurement is essential for measurement of the EW theory precisely.

Polarisation is measured by two independent detectors, the Longitudinal Polarimeter (LPOL) and the Transverse Polarimeter (TPOL). The LPOL is located at between the HERMES spin rotators and the TPOL is located at near the West hall.

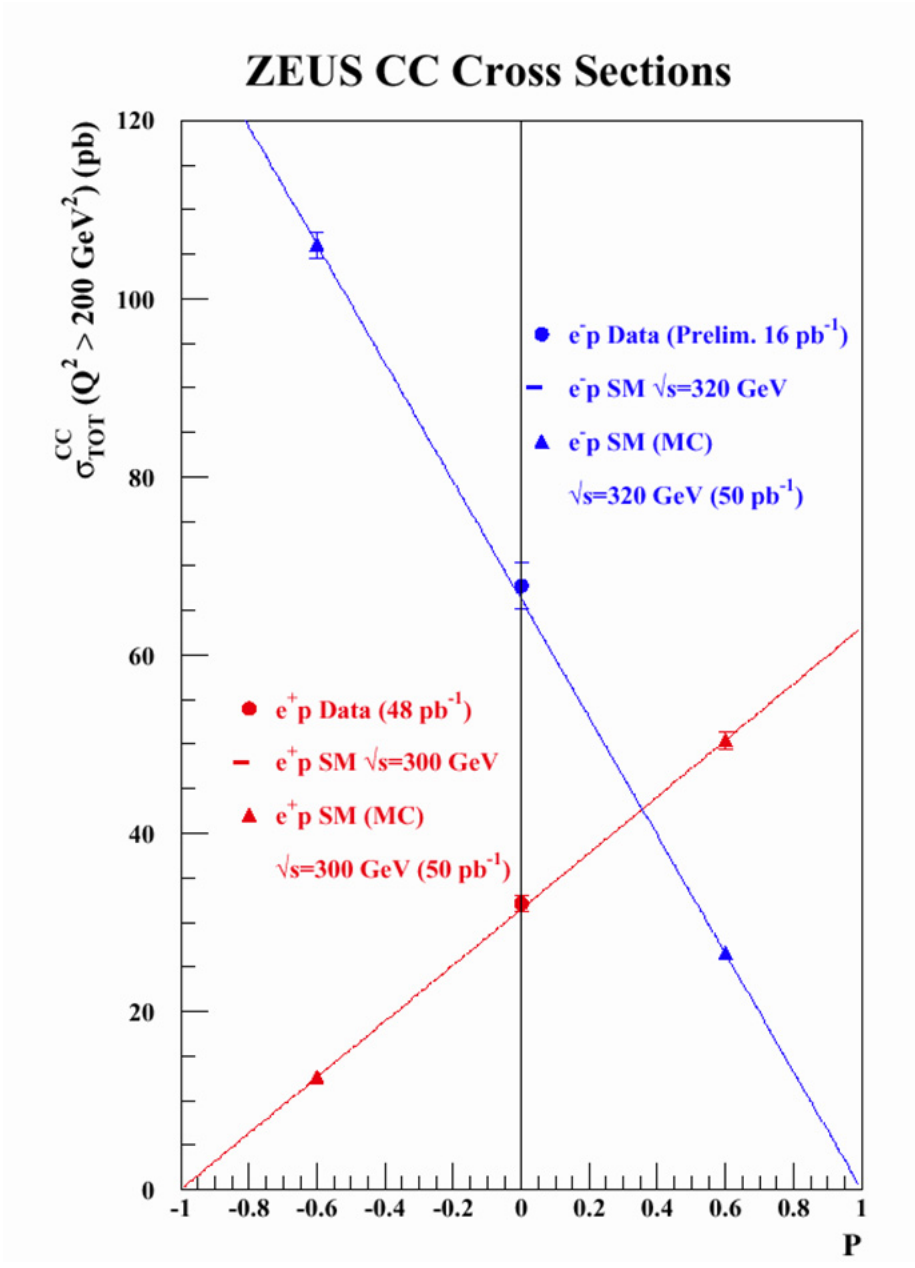


Figure 1.3: Charged Current Cross Section measured at ZEUS against lepton beam polarisation. Blue line indicates the expected value with using electron as a lepton beam and red line is with using positron. Circle points are measurement and triangle are expected from MC.

HERA Reduced NC cross section

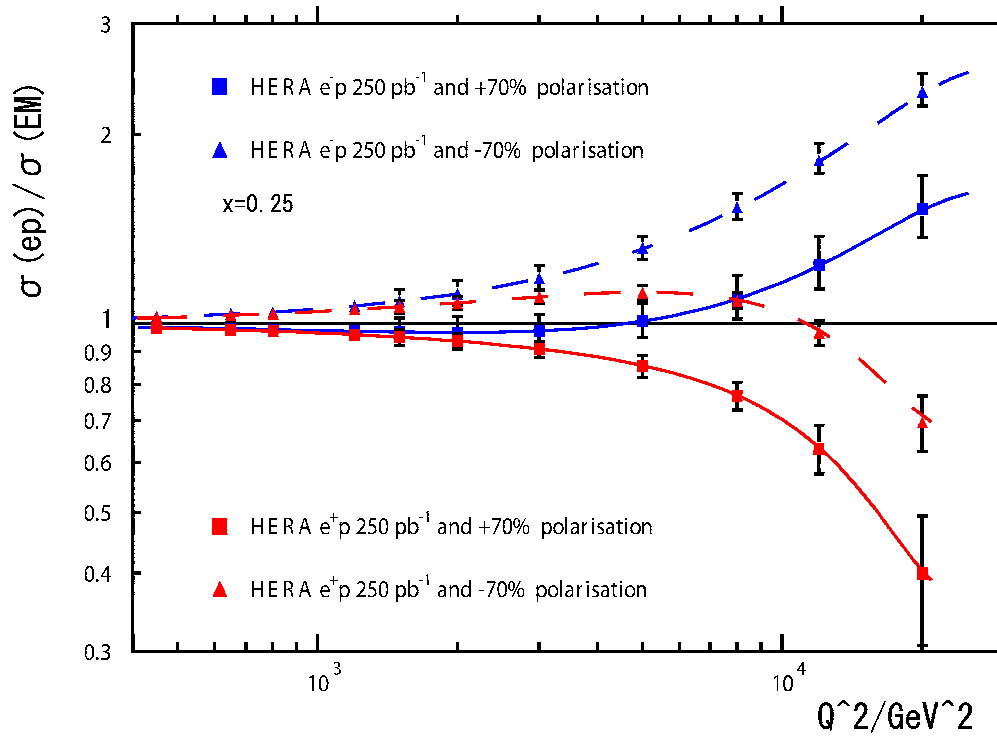


Figure 1.4: The ratio of Neutral Current Cross Section expected by MC and calculated based on the electromagnetic force. Blue line indicates the expected value with using electron as a lepton beam and red line is with using positron. Square points are expected value with +70% polarisation and triangle are expected with -70% polarisation.

The measurement of the polarisation is required with a precision of 2%¹ for physics, which are mentioned above. For that, the TPOL was upgraded in two points during the shutdown, one was that new detectors have been installed, another was that a new DAQ system has been created. And also, analysis method has been upgraded.

In this paper, we present the measurement of lepton beam polarisation. The analysis is based on the whole data from October 2003 to August 2004. In chapter 2, we describe our experimental set up for the TPOL. The principle of polarisation measurement is presented in chapter 3. An overview of the method used for the polarisation measurement is described in chapter 4. The systematic uncertainties on our measurement are discussed and evaluated in the chapter 5 and the results are presented in the chapter 6. Our conclusion is expressed in the chapter 7.

¹Based on some studies; i.e. HERA luminosity, systematic errors and maximum value of the lepton beam polarisation.

Chapter 2

The Transverse Polarimeter

In this chapter, the experimental set up for the transverse polarimeter will be explained.

2.1 The Transverse Polarimeter

The Transverse Polarimeter (TPOL) are consisted of three subdetectors: the calorimeter, the silicon detector and the fibre detector. Each component will be described in the next subsections. Figure 2.1 and Figure 2.2 show the outward of the TPOL and the schematic layout of the three detectors.

TPOL is located at 65m down stream from the interaction point (IP), where a lepton beam collides with the laser light. A linearly polarised laser light is created by an Argon-Ion laser at 9th floor of the West Hall. The polarisation state of the laser can be switched by a Pockel's Cell with a frequency of 90Hz. The energy of the laser light is 2.41eV, which corresponds to a wavelength (λ) of 514.5nm, and the power of the laser light is 10W. Various mirrors, some of them are adjustable, guide the laser light into the HERA tunnel keeping its polarisation to linearly polarised to avoid the degradation of polarisation. The polarisation of the laser light is changed into circularly polarised by a quarter-wave ($\lambda/4$) plate in front of the entrance window. The crossing angle between the lepton beam and the laser light is 3.1 mrad at the IP. After colliding, backscattered photons travel together with scattered lepton, and the dipoles of the next arc bend only the leptons away from the photons. In Figure 2.3, the TPOL optical system is displayed. The procedure of the measurement is as follows. The laser light is closed by a



Figure 2.1: The TPOL outside.

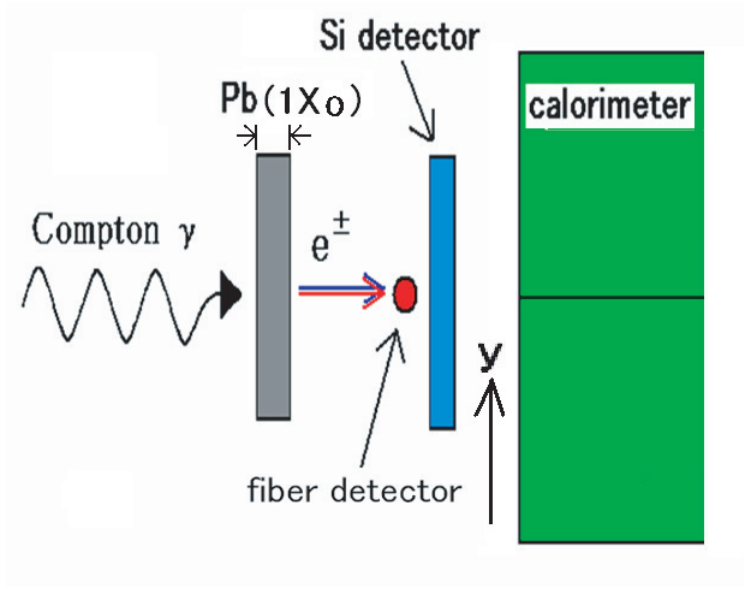


Figure 2.2: The TPOL.

shutter for 20 seconds and then the shutter is opened for 40 seconds. These data recorded during this period are called “laser-off” and “laser-on”, respectively. The laser-off includes bremsstrahlung backgrounds and can be used to subtract them. During the data taking, the circular polarisation of the laser light is changed left- and right-handed by the Pockel’s Cell with a frequency of 90Hz. The data recorded with the laser left-handed helicity is called “laser-left”, and with right-handed is called “laser-right” as well.

2.2 The Calorimeter

The TPOL calorimeter is a sampling calorimeter and is made up of 12 layers. Each layer has a single absorber plate (DENSIMET17, $60 \times 55 \times 6.2 \text{ mm}^3$, $1.6X_0$) and two scintillator plates (SCSN-38, $120 \times 100 \times 2.6 \text{ mm}^3$) which are optically decoupled up and down. Conceptually, the calorimeter can be considered to consist of two calorimeters, one on top of the other; i.e. an UP and a DOWN calorimeter module. The tungsten plates are $60 \times 55 \text{ mm}^2$ and are set in lead frames of $120 \times 100 \text{ mm}^2$. In Figure 2.4, the TPOL calorimeter is displayed. The calorimeter has 4 photomultipliers. The scintillation

Transverse Polarimeter

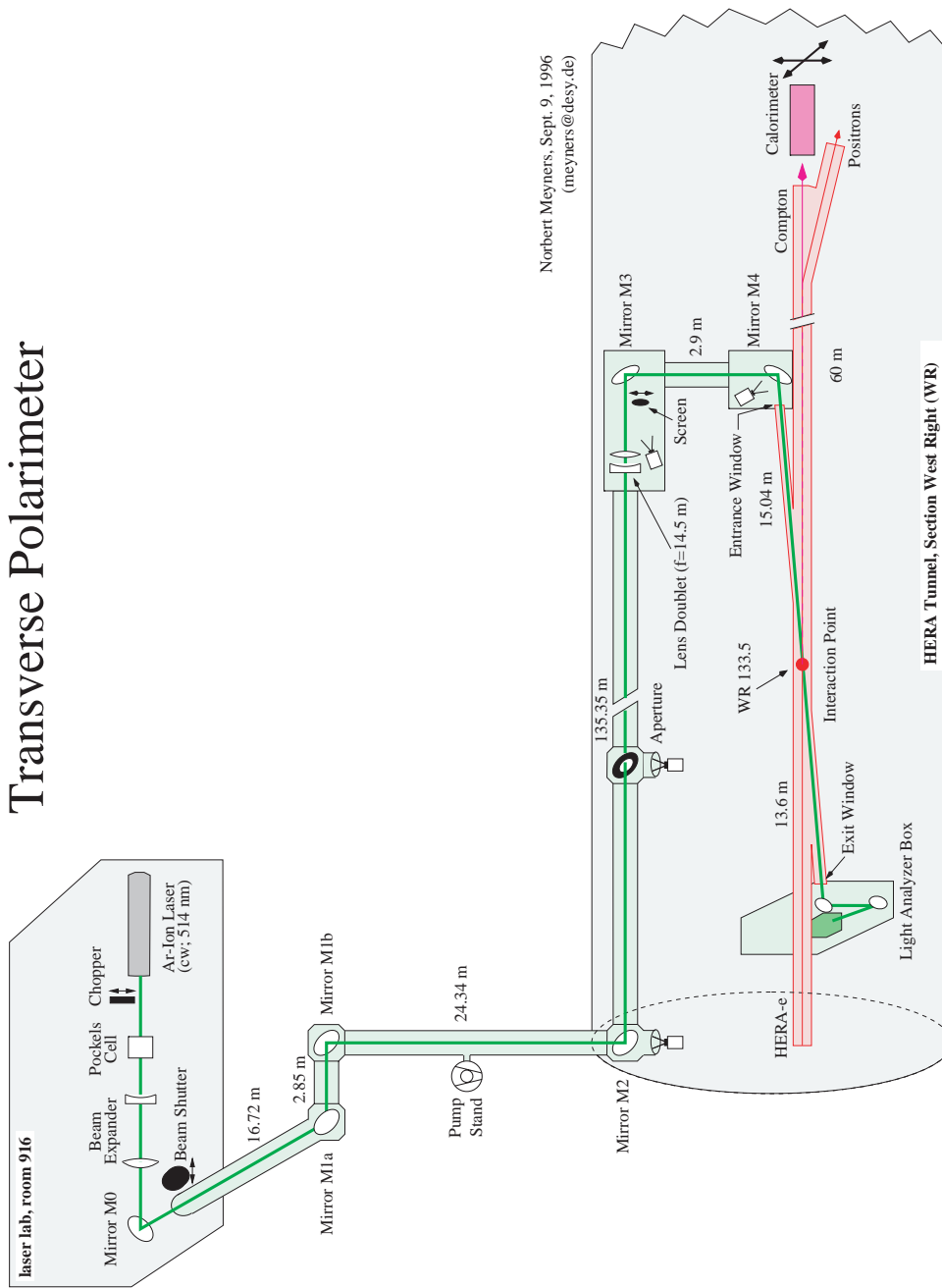


Figure 2.3: TPOL optical system.

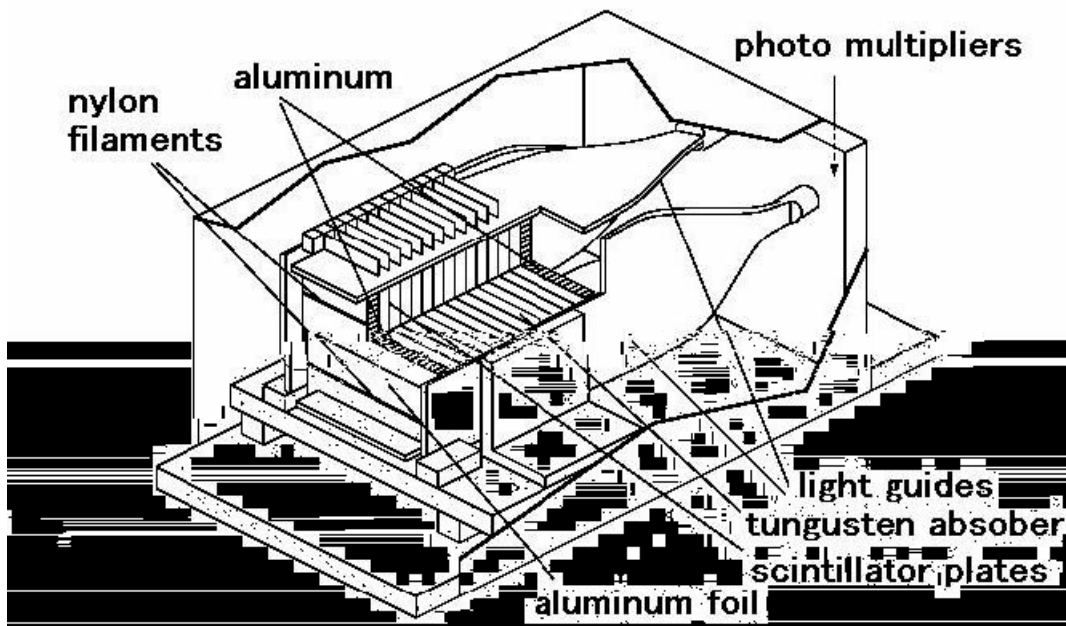


Figure 2.4: TPOL Calorimeter

light, which is created in the scintillator plate when charged particles enter is collected and feeded to the photomultipliers through Wave Length Shifters (WLS)s, which are fixed to each side of the calorimeter. The WLS is made of an acrylic plate doped with a fluorescent material commercially called Y-7. The energy of incoming photon is measured as a sum of the energy in the two halves:

$$E_\gamma = E_U + E_D. \quad (2.1)$$

Two dimensional histograms of the total energy and its asymmetry of the photons are piled for “laser-left”, “laser-right” and “laser-off” separately. In Figure 2.5, the histograms are shown. The left column shows laser-left, the right shows laser-right. The calibration of the calorimeter is done by adjusting four PMT’s voltages. The relative calibration of channels L and R is done by measuring the horizontal energy asymmetry $\eta_H(x)$:

$$\eta_H(x) = \frac{E_L - E_R}{E_L + E_R}. \quad (2.2)$$

If two channels are properly calibrated, the horizontal energy asymmetry should be 0. For the calibration of the vertical channels, a ratio of sum of the vertical energy and a sum of the horizontal energy is used. The ratio is defined as:

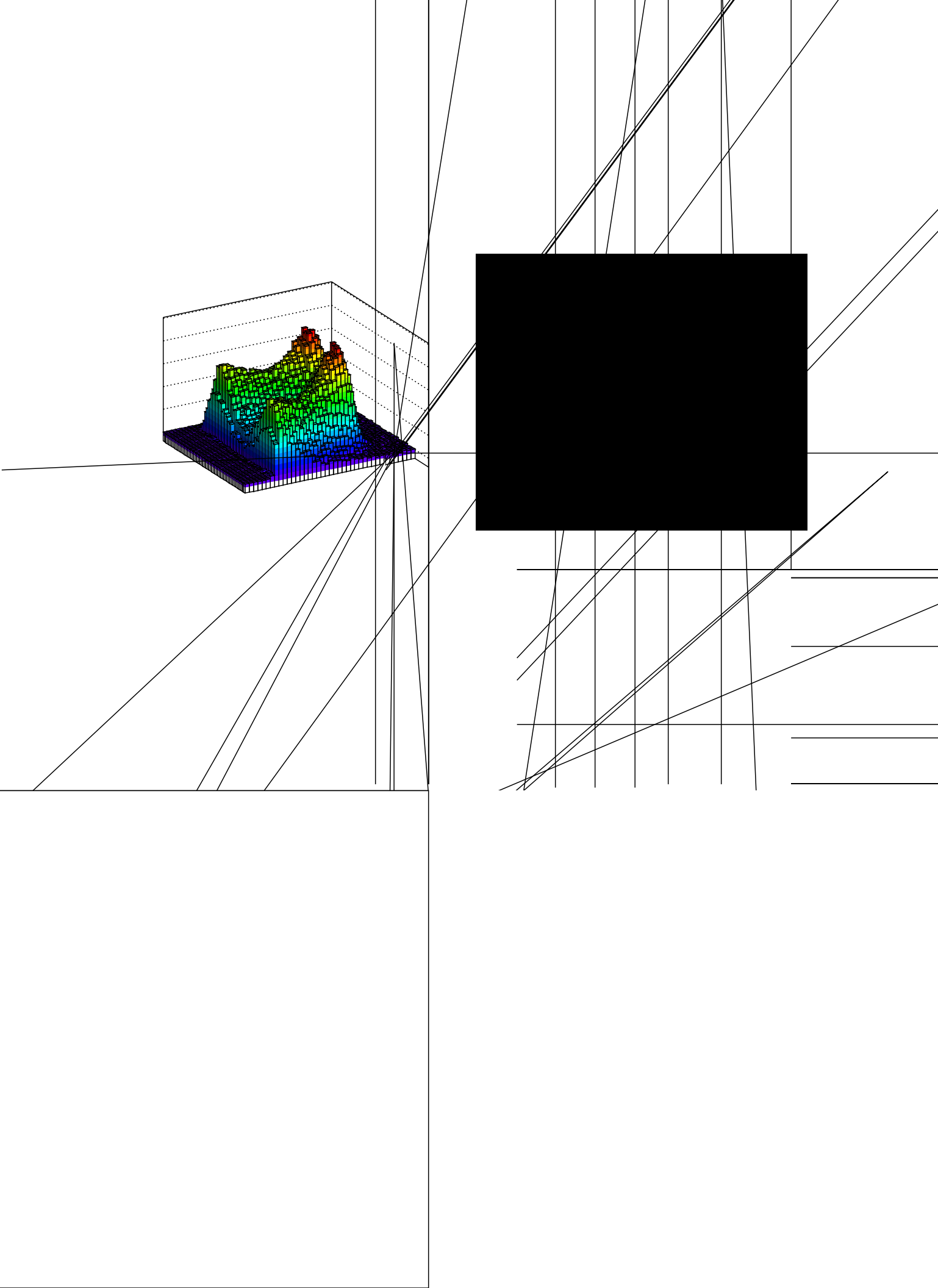
$$R = \frac{E_V}{E_H} = \frac{E_U + E_D}{E_L + E_R}. \quad (2.3)$$

Apart from small effects due to light attenuation in the scintillator, this ratio should be 1 independent of the incoming particle position and its energy. Then, it is assumed that at the centre of the calorimeter $R=1$. The calorimeter does not measure a vertical position of Compton photon directly, but the vertical energy asymmetry $\eta_V(y)$ can be used as a measurement of the vertical position. It is defined as:

$$\eta_V(y) = \frac{E_U - E_D}{E_U + E_D}. \quad (2.4)$$

An vertical energy asymmetry $\eta_V(y)$ which is measured in the calorimeter is transformed to the vertical position(y) with using an “ η - y transformation”. This transformation formula is defined as:

$$y(\eta) = P1(\log \frac{1+\eta}{1-\eta}) + P2(\log \frac{1+\eta}{1-\eta})^3 + P3(\log \frac{1+\eta}{1-\eta})^5 + P4(\log \frac{1+\eta}{1-\eta})^7, \quad (2.5)$$



where η is same as η_V and hereafter η will be used instead of η_V . A vertical position is also measured by the silicon detector, which will be presented in next section.

2.3 The Silicon Detector

2.3.1 The Silicon Detector

The silicon detector is a position sensitive microstrip detector and has been installed in front of the calorimeter. It consists of two pieces of sub-silicon detectors, which measure horizontal X-position and vertical Y-position of an incoming backscattered Compton photon. The Y-silicon detector is a Hamamatsu ATLAS prototype: $64 \times 63.6 \text{ mm}^2$ and $300 \mu\text{m}$ thick. It consists of 768 strips $80 \mu\text{m}$ pitch, and a position resolution is $24 \mu\text{m}$. The X-silicon detector is a Hamamatsu ZEUS MVD: $64 \times 63.6 \text{ mm}^2$ and $300 \mu\text{m}$ thick. It consists of 256 strips $120 \mu\text{m}$ pitch and read out every other one strip. These two detectors are readout by 6 APV25 amplifier/multiplexer chips. The Y-silicon detector is located downstream with regard to the X-silicon detector in order to measure the vertical position of backscattered Compton photon as precisely as possible to get a good η - y transformation. In Figure 2.6 and Figure 2.7 the silicon detector is displayed.

These detectors have been added for the TPOL up-grade during shut-down from HERA I to HERAII. At HERA I, the η - y transformation was the biggest source of systematic uncertainty for the polarisation measurement, the error amounted to around 4%¹. In order to reduce this error, vertical position of the backscattered photons is necessary to measure precisely. For that reason, the silicon detector has been installed at HERAII and has been used for the *in-situ* calibration. As mentioned before, the precision of polarisation measurement required for high-luminosity HERAII physics is under 2%. Because the silicon detector can detect only charged particles not neutral particles like photon, a pre-radiator of one radiation length of lead has been placed a few centimetres in front of the detector. A photon is converted into charged particles, electron and positron, then these charged particles hit the silicon detector. The read out rate of the DAQ of the silicon detector is around 100Hz and far slower than that of calorimeter².

¹Also explained in section 3.3.

²100kHz

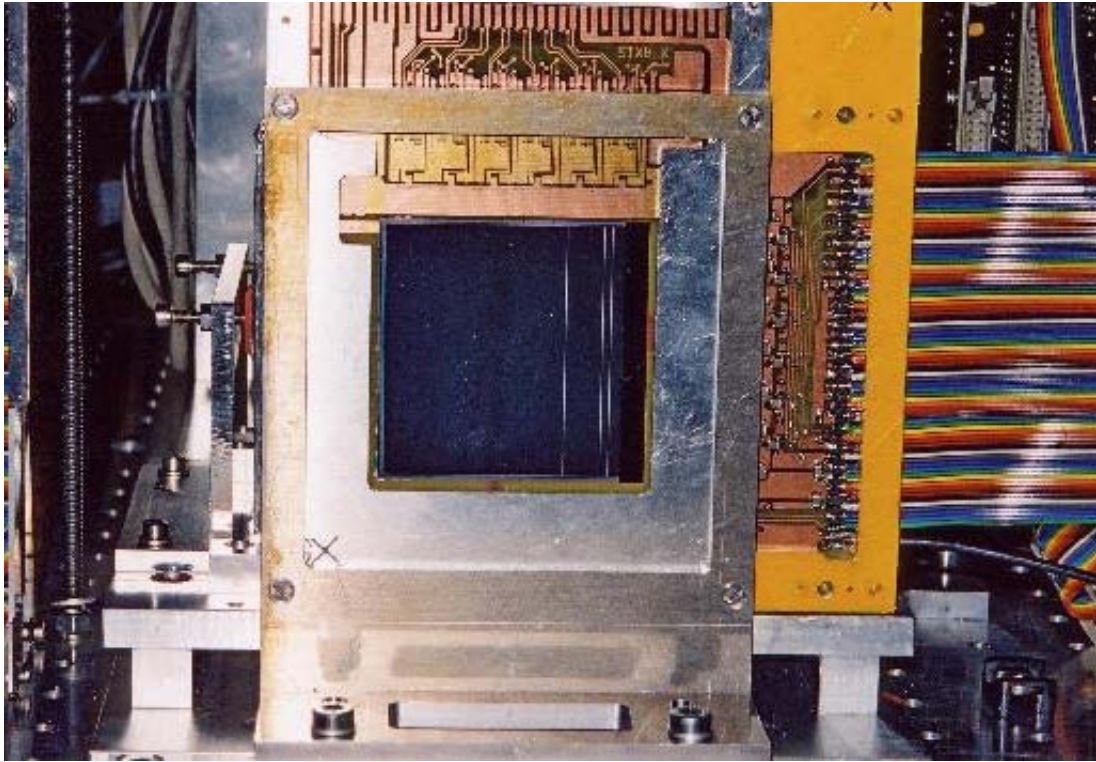


Figure 2.6: Front view of the silicon detector

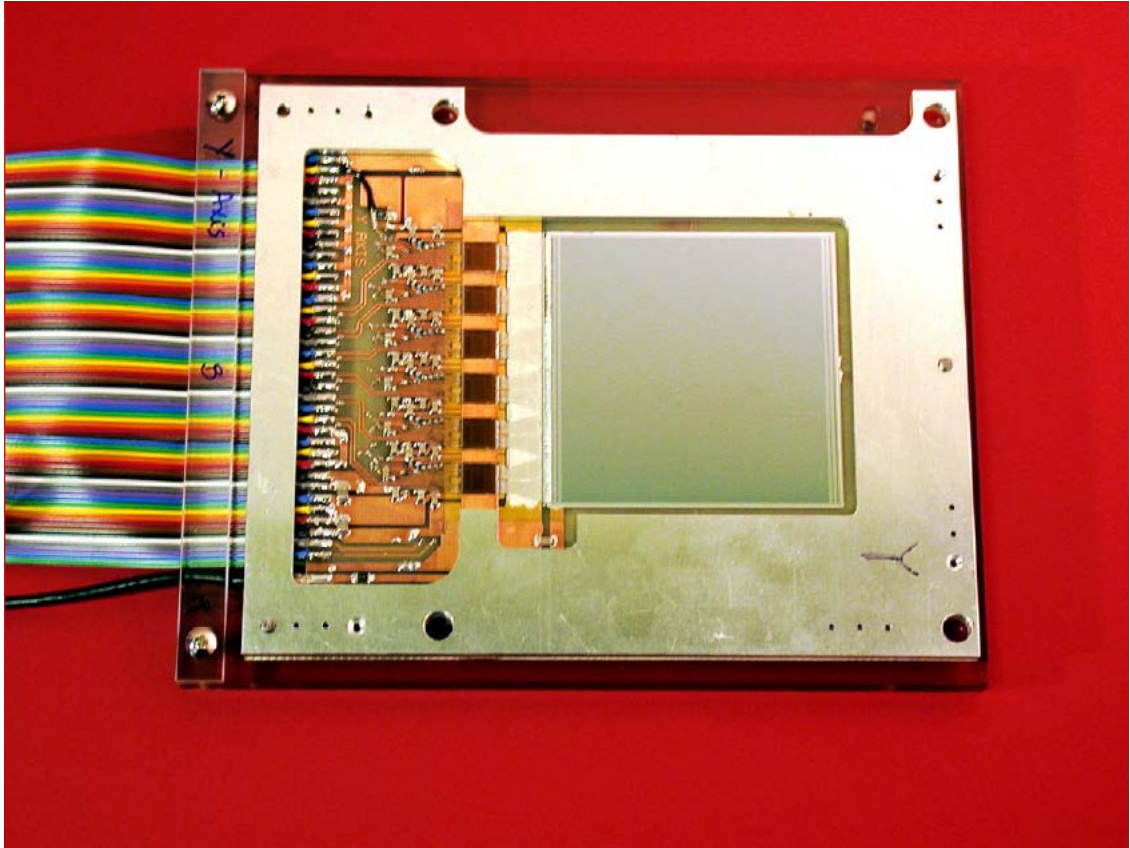


Figure 2.7: A piece of the sub-silicon detector

2.3.2 Clustering Algorithm

Before describing the algorithm, the definition of some variables used to calculate the cluster is explained below.

- **Strip Pulse Height PH_i**

The pulse height is calculated with the following equation:

$$PH_i = ADC_i - PED_i - CM, \quad (2.6)$$

where:

ADC_i =raw ADC counts in strip i ;

PED_i =mean pedestal value in ADC counts;

CM =Common Mode baseline shift correction for each event.

- **Strip Noise N_i**

The noise of a given strip is calculated as the root mean square (RMS) of PH_i :

$$N_i = RMS(PH_i). \quad (2.7)$$

The silicon cluster algorithm goes through the following steps listed below.

- Scan the 768 strips to find the cluster seeds. The condition of the cluster seed selection is:

$$PH_i > 5 * N_i. \quad (2.8)$$

- Scan the strips around the cluster seed. Strips with $PH_i > 3 * N_i$ will be included in the cluster.
- Calculate distance between the different cluster seeds. If there are less than 6 strips between two seeds, these clusters are considered to belong to the same cluster, otherwise, considered to be different cluster.

2.4 The Fibre Detector

The fibre detector is also a position sensitive detector and has been installed about 1cm upstream from the silicon detector. The purpose for setting this detector is to calibrate the linearity of the response of the silicon detector and to monitor the degradation of the silicon detector due to the radiation dose to

it. Since the expected radiation dose has been estimated to 1.9Mrad/year[4], it is expected that the silicon detector will be damaged and this damage may cause a uncertainty to the polarisation measurement. The fibre detector consists of the scintillating fibre (KURARAY,SCSF-81M) whose length and diameter are 70mm and 1mm, respectively, and clear fibres (Edmund Scientific Japan., Ltd) which are connected to two PMTs at the both side of the scintillating fibre. A scintillation light emitted in the fibre is transmitted to two PMTs through the clear fibres. The fibre detector is fixed to the aluminium support plate and moved by a stepping motor. The precision of the stepping motor is $1\mu\text{m}$. A study about how uncertainty should be estimated by the radiation dose to the silicon detector has been done[5]. In Figure 2.8, the picture of fibre detector are shown.

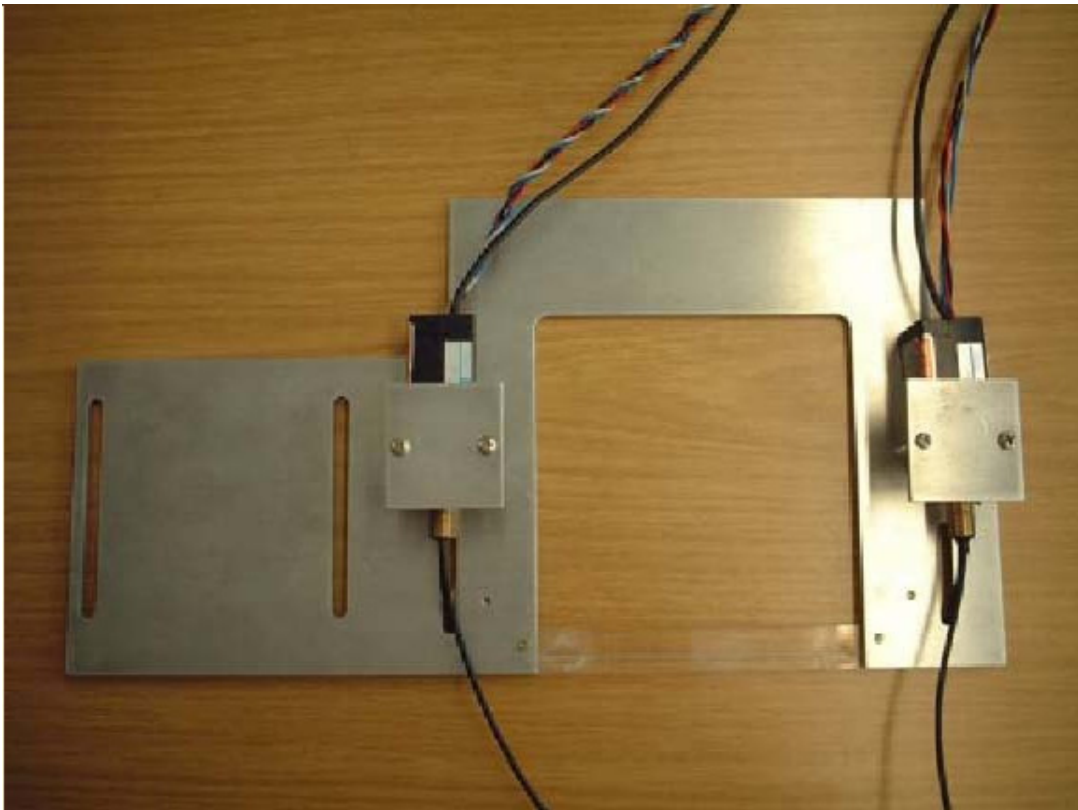


Figure 2.8: The Fibre Detector

2.5 The η - y transformation

In this section, the determination of the η - y transformation will be described. Actually, there exists some systematic uncertainties in the polarisation measurement. Among these uncertainties, the precision of the η - y curve³ measurement causes a large systematic uncertainty to the polarisation measurement as mentioned in section 2.3. Therefore, a careful determination is needed. The $\eta(y)$ variable is obtained from the calorimeter measurement (See Eq.(2.4)). The y variable is the vertical hit position of the backscattered photon and is obtained from the Y-silicon detector. For deriving the η - y curve, we have used two methods. One is the “Normal mode”, and the another is the “Table scan mode”.

Usually, when the calibration of the η - y curve⁴ is executed, data taking mode is called “Normal mode”. The backscattered photon is entering around the centre of the calorimeter. Therefore, in the Normal mode, the number of particles entering the silicon detector is small in the region far from the centre and due to the pre-radiator in front of the silicon detector, there are some particles entering the silicon detector with some angle. As a results, these two facts may cause bias in deriving the η - y curve.

To make up the small number of event at large η region and to reduce the events that particles enter the silicon detector with some angles, the table on which the calorimeter is moved along the vertical direction, up and down⁵ As a results, the beam profile on the Y-silicon detector can be almost flat along the vertical direction and probably the bias can be suppressed. This data taking mode is called “Table scan mode”. Actually, there may exist possibility to have the bias for extracting the η - y curve in the Normal mode, but at present we can not answer the question why the difference of beam profile causes the bias to the curve⁶ In this analysis, therefore, the Normal mode will be used to extract the η - y curve. Then, the η - y curve extracting from the Table scan mode will be included as a systematic uncertainty.

³It is a curve used for the transformation.

⁴This calibration means that y variable is measured by the silicon detector and the η - y curve is calibrated, not for the calibration of the calorimeter.

⁵The table is moved together with the silicon detector and the fibre detector.

⁶To clear this question, a MC is necessary. But, unfortunately we do not have one at present.

2.6 The procedure of deriving the η - y curve

The determination procedure of the η - y curve is as follows.

1. Create an η - y scatter plot by requiring two kinds of selection cut, i.e. only one cluster event in the Y-silicon detector and the energy of the calorimeter is greater than 5 GeV. The η - y plot is displayed in Figure 2.9.
2. Slice the scatter plot in η from -1 to 1 with 0.05 interval .
3. Fit the y distribution in each η slice with a Gaussian, but the data used only between a region $\pm 2\text{RMS}$ around the mean⁷.
4. Again, fit the same distribution with a Gaussian with the data only between a region $\pm 2\text{RMS}$ around the mean obtained by filling as above.
5. Repeat procedures 4 until the difference between those two means is less than 0.01. Then, Eq.(2.5) fits points obtained above and the η - y curve is determined.

Figure 2.10 and 2.11 show two kinds of η - y curves which are created according to above procedure. These procedures are in common with two data taking mode. Also, in Figure 2.12 shows the η - y curves from the Normal mode and the Table scan mode. It is seen that there is a discrepancy in the high η region.

⁷This is not a Gaussian mean.

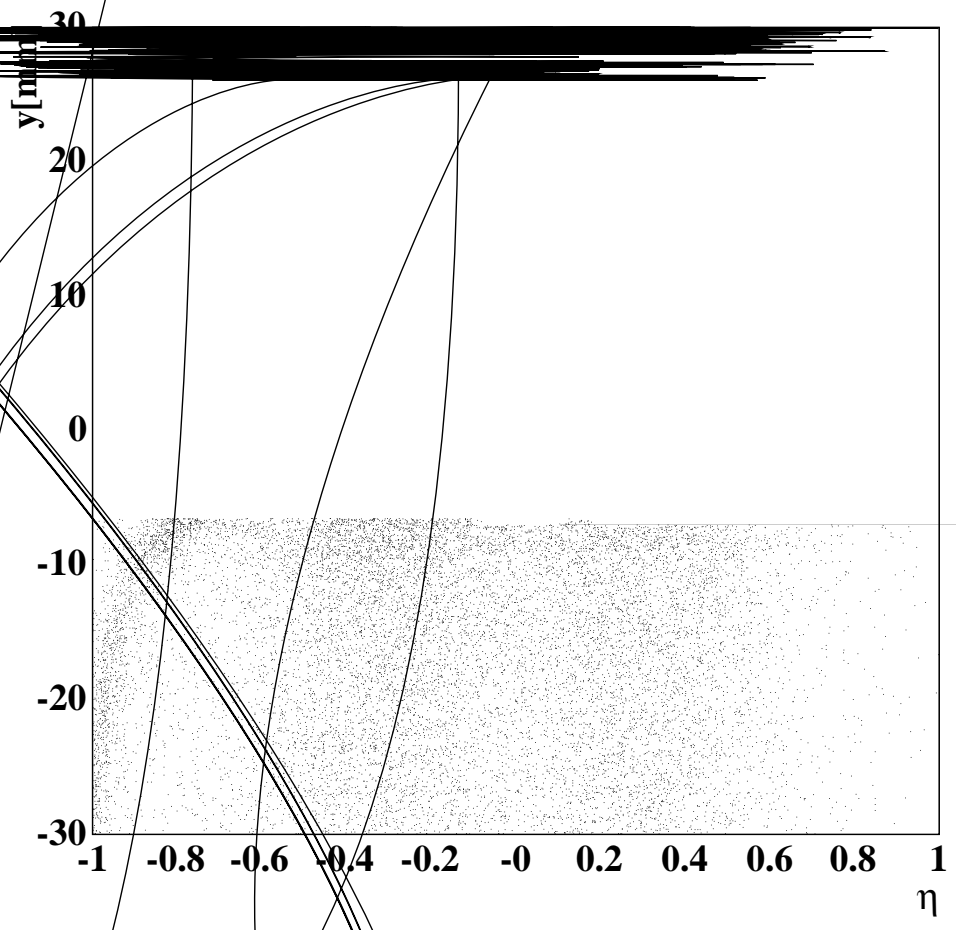


Figure 2.9: The η - y scatter plot. That y is equal to 0 corresponds to the centre of the calorimeter.

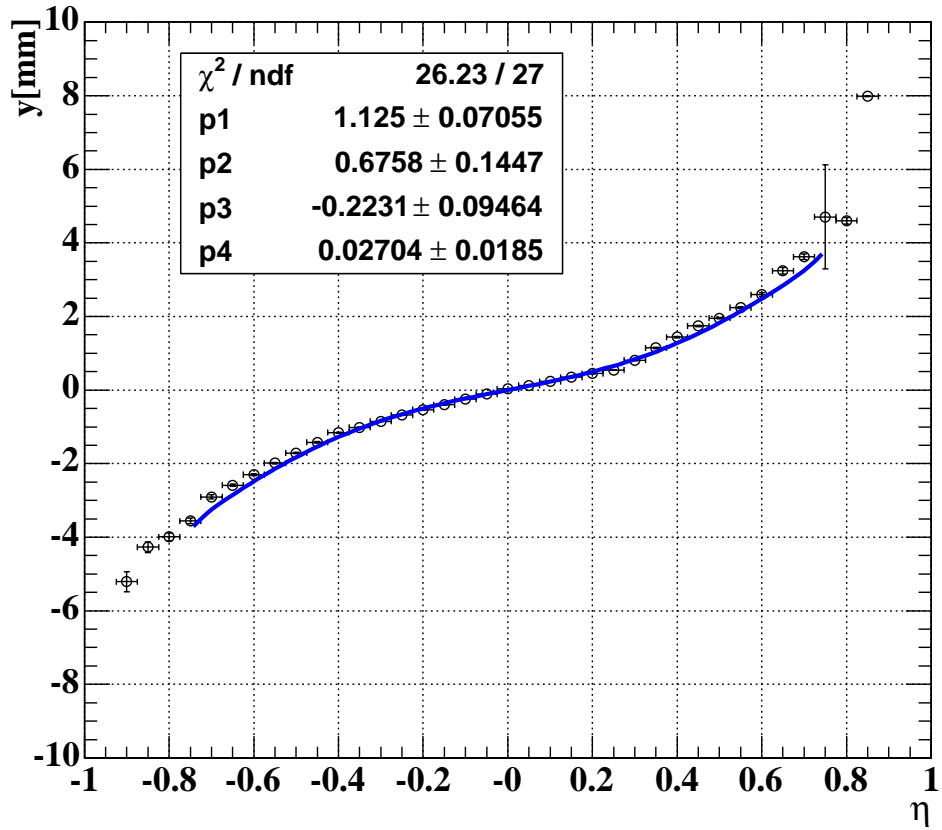


Figure 2.10: The η - y curve with the Normal mode

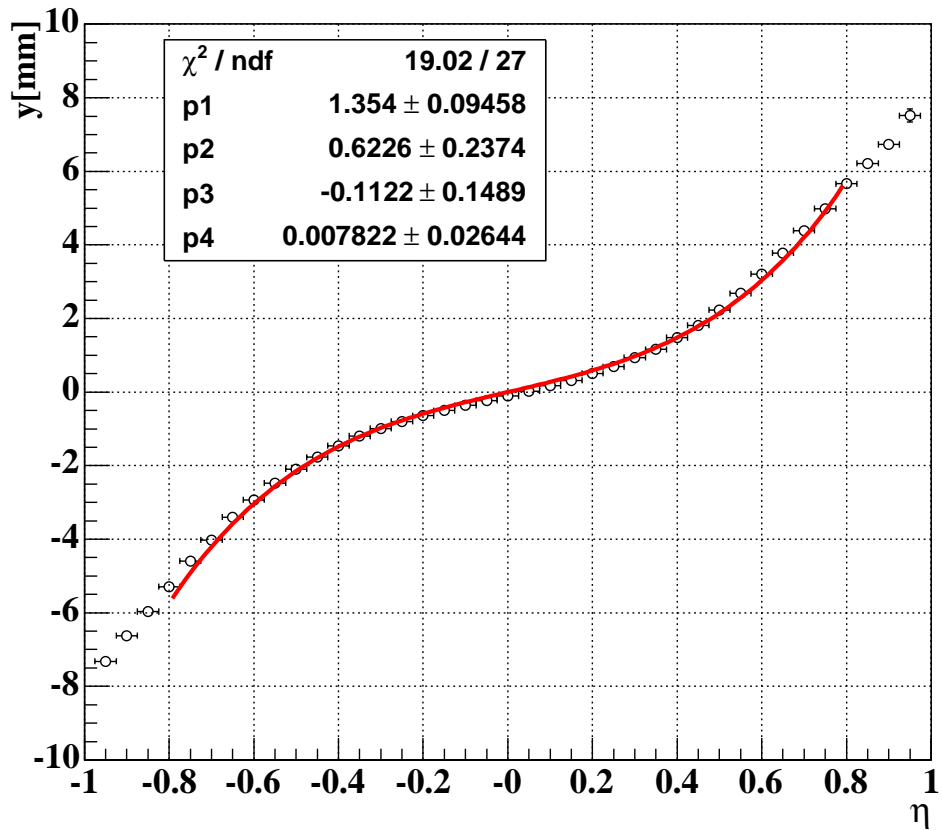


Figure 2.11: The η - y curve with the Table scan mode

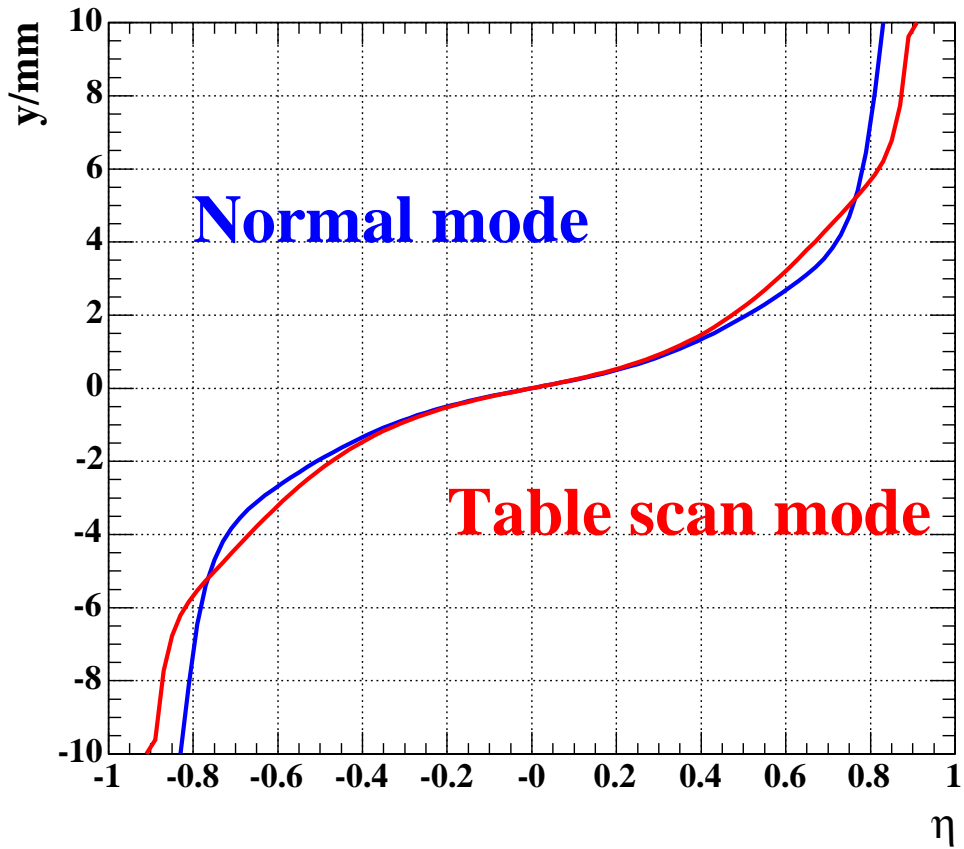


Figure 2.12: Comparison with two η - y curves

Chapter 3

Polarisation Measurement

In this chapter, a method of polarisation measurement will be explained.

3.1 Polarisation at HERA

A spin of lepton beam in the HERA storage ring can be transversely polarised through the Sokolov-Ternov effect[6]: the probability of spin flipping from up to down and from down to up is not equal because of the synchrotron radiation in the magnet field. The spin rotator can change the lepton beam's spin from transverse to longitudinal, and the longitudinal polarised lepton beam collides with a proton beam at the ZEUS and H1 detectors. The polarisation of lepton beam increases in time gradually according to the following formula:

$$P(t) = P_{max}(1 - e^{-t/\tau}), \quad (3.1)$$

where P_{max} is the asymptotic polarisation and τ is the build-up time and $P(0)$ is assumed to be 0. If the magnet field is uniform in the storage ring, the asymptotic polarisation is maximum: $P_{max} = P_{ST} = 92.4\%$ and τ is τ_{ST} where τ_{ST} and P_{ST} mean the Sokolov-Ternov build-up time and its polarisation, respectively. But in actual due to some depolarisation effects (magnet misalignments, non-uniform magnet field), the polarisation is rather suppressed. If these depolarisation effects are depicted as a constant τ_D , the asymptotic polarisation P_{max} can be written as:

$$P_{max} = P_{ST} \frac{\tau_D}{\tau_{ST} + \tau_D}. \quad (3.2)$$

Also, the build-up time τ can be written as

$$\tau = \tau_{ST} \frac{\tau_D}{\tau_{ST} + \tau_D}. \quad (3.3)$$

At HERA, τ_{ST} is 37 min for 27.5 GeV lepton beam. For example, at 27.5 GeV, with $\tau_D = 10 \text{ min}^1$, the build-up time is 8 min. With this build-up time and Eq.(3.2), the P_{max} can be calculated. This allows us an absolute scale calibration of the polarisation measurement by comparing the measured asymptotic polarisation to the P_{max} predicted from the measured build-up time.

3.2 Compton scattering

Polarisation of lepton beam can be measured using Compton scattering. Figure 3.1 shows the process of Compton scattering in the laboratory frame and the lepton rest frame. In that picture, k_i and k_f denote a momentum of incident laser light and a momentum of scattered photon in the rest frame, respectively. At TPOL of HERA, $k_i = 0.508$. The rest frame and the laboratory frame are correlated each other as follows:

$$k_i = 2\gamma E_\lambda / m_e = 2E_e E_\lambda / m_e^2, \quad (3.4)$$

$$k_f = 1 / (1 - \cos \theta_{lab} + 1/k_i), \quad (3.5)$$

where θ_{lab} is a scattering angle in the lepton rest frame and it depends only on the energy of photon in the laboratory frame. E_e is an energy of the incident lepton, E_λ is an energy of incident laser in the laboratory frame and m_e is the lepton mass, respectively. γ is the Lorentz boost factor to the rest frame. Therefore, photons with same energy can be observed on the surface of a detector with concentric circle:

$$\cos \theta_{lab} = \frac{E_e - E_\gamma(1 + 1/k_i)}{E_e - E_\gamma}, \quad (3.6)$$

where E_γ means the energy of backscattered photons in the laboratory frame. Then, a radius of the concentric circle is

$$R(E) = D \tan \theta_{lab} = \frac{D}{\gamma \tan \theta/2}, \quad (3.7)$$

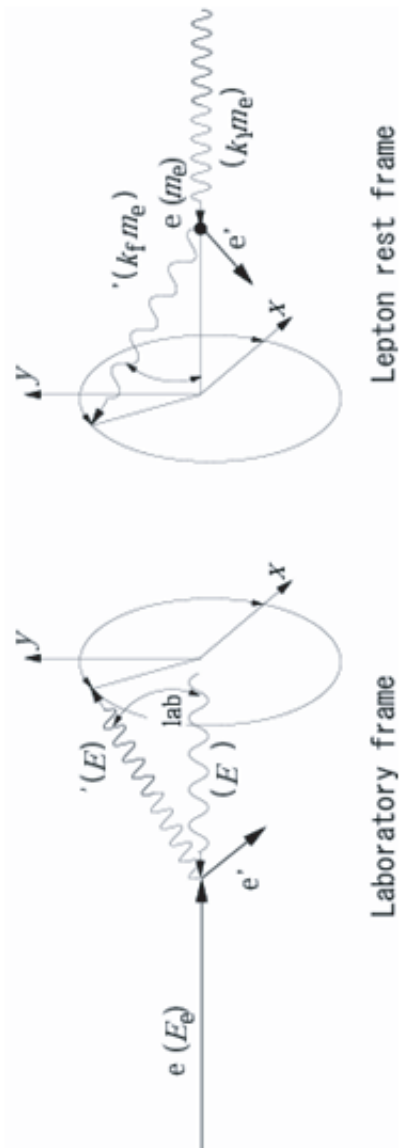


Figure 3.1: Kinematic process of Compton scattering: a laboratory frame is shown in bottom and a lepton rest frame is shown in top.

Quantity	rest frame	laboratory frame
k_i	momentum of incident laser light	
k_f	momentum of scattered photon	
E_λ		energy of incident laser light
E_e		energy of incident lepton
E_γ		energy of scattered photon
θ	scattering angle of photon	
θ_{lab}		scattering angle of photon
m_e		lepton mass
ϕ		azimuthal angle

Table 3.1: Some kinematics variables

where D is the distance from the calorimeter surface to the IP where laser light and lepton beam collide. The azimuthal angle ϕ is connected to the vertical position of the scattered photon if the energy is known:

$$y = R(E_\gamma) \sin \phi. \quad (3.8)$$

Some kinematics variables related to these formulas are shown in Table 3.1. When $\theta = 180^\circ$, an observed energy of photon becomes maximum:

$$E_{max} = \frac{2E_e}{2 + 1/k_i}. \quad (3.9)$$

The polarisation of the initial photon is described using Stokes Vector $\mathbf{S} = (S_0, S_1, S_2, S_3)$ and two electric fields E_1, E_2^2 :

$$S_0 = E_1^2 + E_2^2, \quad (3.10)$$

$$S_1 = E_1^2 - E_2^2, \quad (3.11)$$

$$S_2 = 2E_1E_2 \cos \delta, \quad (3.12)$$

$$S_3 = 2E_1E_2 \sin \delta, \quad (3.13)$$

where δ is the angle between the two electric fields. By definition S_1 and S_2 are related to the linear polarisation S_{lin} as:

$$S_{lin} = \sqrt{S_1^2 + S_2^2}. \quad (3.14)$$

¹ τ_{ST} is constant under the 27.5GeV lepton beam at HERA and τ can be measurable. Thus, τ_D can be determined from the Eq.(3.3).

²electric field and magnetic field.

And S_3 is the circular polarisation of the laser light and is connected with linear polarisation as:

$$S_{circ} = \sqrt{1 - S_{lin}^2} = S_3. \quad (3.15)$$

If the helicity of the laser light is right-handed, S_3 is defined as $S_3 < 0$ and in case of left-handed $S_3 > 0$. The polarisation of the initial lepton is described in Cartesian coordinates by $\mathbf{P} = (P_X, P_Y, P_Z)$. Then, the differential Compton cross section can be written as:

$$\frac{d\sigma}{d\Omega}(\mathbf{S}, \mathbf{P}) = \Sigma_0 + S_1(0)\Sigma'_1 + S_3(P_Y\Sigma_{2Y} + P_Z\Sigma_{2Z}), \quad (3.16)$$

where $\Sigma_0, \Sigma'_1, \Sigma_{2Y}$ and Σ_{2Z} can be written as follows:

$$\Sigma_0 = C[(1 + \cos^2 \theta) + (k_i - k_f)(1 - \cos \theta)], \quad (3.17)$$

$$\Sigma'_1 = C \cos 2\phi \sin^2 \theta, \quad (3.18)$$

$$\Sigma_{2y} = -Ck_f \sin \phi \sin \theta (1 - \cos \theta), \quad (3.19)$$

$$\Sigma_{2z} = -C(1 - \cos \theta)(k_f + k_i) \cos \theta. \quad (3.20)$$

The factor C is given:

$$C = \frac{r_0^2 k_f^2}{2k_i^2}, \quad (3.21)$$

where $r_0 = 2.818 fm$ is the classical electron radius. The polarisation can be obtained by comparing two different laser light states $\mathbf{S}_a = (S_{0a}, S_{1a}, S_{2a}, S_{3a})$ with $\mathbf{S}_b = (S_{0b}, S_{1b}, S_{2b}, S_{3b})$. For example, the cross section asymmetry between two laser light states:

$$A = \frac{\sigma_a - \sigma_b}{\sigma_a + \sigma_b}, \quad (3.22)$$

where σ_a, σ_b are the cross sections of laser light state in $\mathbf{S}_a, \mathbf{S}_b$, respectively can be rewritten as follows with Eqs.(3.16),(3.17),(3.18),(3.19),(3.20):

$$A = \frac{\Delta S_1 \Sigma'_1 + \Delta S_3 [P_Y \Sigma_{2y} + P_Z \Sigma_{2z}]}{\Sigma_0 + \bar{S}_1 \Sigma'_1 + \bar{S}_3 [P_Y \Sigma_{2y} + P_Z \Sigma_{2z}]}, \quad (3.23)$$

where $\Delta S_1 = (S_{1a} - S_{1b})/2, \Delta S_3 = (S_{3a} - S_{3b})/2, \bar{S}_1 = (S_{1a} + S_{1b})/2, \bar{S}_3 = (S_{3a} + S_{3b})/2$, respectively. If two polarisation states \mathbf{S}_a and \mathbf{S}_b are selected

as $\bar{S}_1 = 0$ and $\bar{S}_3 = 0^3$, this corresponds to the situation which the circular polarisation of the laser light is changing left and right alternately since flipping the helicity of laser light means changing the sign of S_3 and unchanging the sign of S_1 . Then, Eq.(3.23) can be rewritten in more simple formula as follows:

$$A = \Delta S_1 \frac{\Sigma'_1}{\Sigma_0} + \Delta S_3 [P_Y \frac{\Sigma_{2y}}{\Sigma_0} + P_Z \frac{\Sigma_{2z}}{\Sigma_0}]. \quad (3.24)$$

According to the above formula, it is noted that the asymmetry A is proportional to the transverse polarisation P_Y and the longitudinal polarisation P_Z .

3.3 Measurement of Transverse Polarisation

Since the term Σ_{2y} has a $\sin \phi$ dependence (See Eq.(3.19)), Eq.(3.24) can be a function of y . Therefore, assuming $\Delta S_1 = 0$ and $P_Z = 0$ for simplicity, P_Y can be obtained from the shift of the mean vertical position of the backscattered photon when the laser light is switched its polarity left and right. Then, the shift can be written as:

$$\Delta y(E_\gamma) = \frac{\langle y \rangle_L - \langle y \rangle_R}{2} = \Delta S_3 P_Y \Pi_y(E_\gamma), \quad (3.25)$$

where $\Pi_y(E_\gamma)$ is called the Analysing Power and is equal to the shift of y when $\Delta S_3 P_Y = 1^4$. In the TPOL data analysis, the polarisation can be calculated with Eq.(3.25) in principle. However, what the calorimeter can measure is the energy asymmetry η only and the $\eta - y$ transformation is necessary for calculating the polarisation. We have used the formula as follows instead of Eq.(3.25):

$$\Delta \eta(E_\gamma) = \frac{\langle \eta \rangle_L - \langle \eta \rangle_R}{2} = \Delta S_3 P_Y \Pi_\eta(E_\gamma), \quad (3.26)$$

where $\Pi_\eta(E_\gamma)$ is the Analysing Power transformed from $\Pi_y(E_\gamma)$ using the $\eta - y$ transformation. From the above formula, the uncertainty on the measured polarisation can be expressed as:

$$\delta P_Y / P_Y = \delta \Pi_\eta / \Pi_\eta + \dots \quad (3.27)$$

³This implies $\Delta S_1 = 0$ and $\Delta S_3 = 1$.

⁴Usually, estimated by MC and typical value is 0.142 mm.

therefore the Analysing Power, Π_η , dominates the analysis. According to the test beam results[7], the difference between the Analysing Power obtained at DESY and that obtained at CERN(Centre Européen de Recherche Nucléaire) can be as large as 4.4%. This is significantly larger than our goal of $\delta P/P \leq 0.02$. In order to reduce the systematic uncertainty due to the η - y transformation, the silicon detector has been installed and used to calibrate the η - y transformation. Thus, we can measure the y position directly by the silicon detector and typically the measured Δy is 0.03 mm at $P = 24\%$.

However, as described before the speed of the DAQ of the silicon detector is slower than that of the calorimeter and the statistical error seems to be large. Therefore, we have calculated the polarisation using Eq.(3.26) not Eq.(3.25). This is a standard way to measure P_Y and called “The averaging method”. This method has been adopted to the online measurement of the lepton beam polarisation. In this online analysis, the averaged η value is calculated in the energy range of $5.2 \text{ GeV} < E_\gamma < 11.4 \text{ GeV}$, where the cross section is most sensitive to the polarisation. In Figure 3.2, some histograms used for the averaging method are displayed. In that picture, the data enclosed by the red box is used for the averaging method. As an advantage of this method, the polarisation value can be calculated real time for monitoring purposes.

On the other hand, there actually exists a disadvantage in the averaging method. In this method, various conditions related to the lepton beam and the calorimeter are treated as unchangeable. For example, following conditions are assumed to be constant implicitly:

- the vertical offset between the Compton beam and the centre of the calorimeter
- the vertical width of the lepton beam at the IP
- the vertical width of the Compton beam on the calorimeter surface (called “focus size”)
- the energy resolution of the calorimeter
- the η - y transformation
- the linear component of the laser light polarisation⁵

⁵ ΔS_1 is assumed to be 0 and ΔS_3 is to be 1.

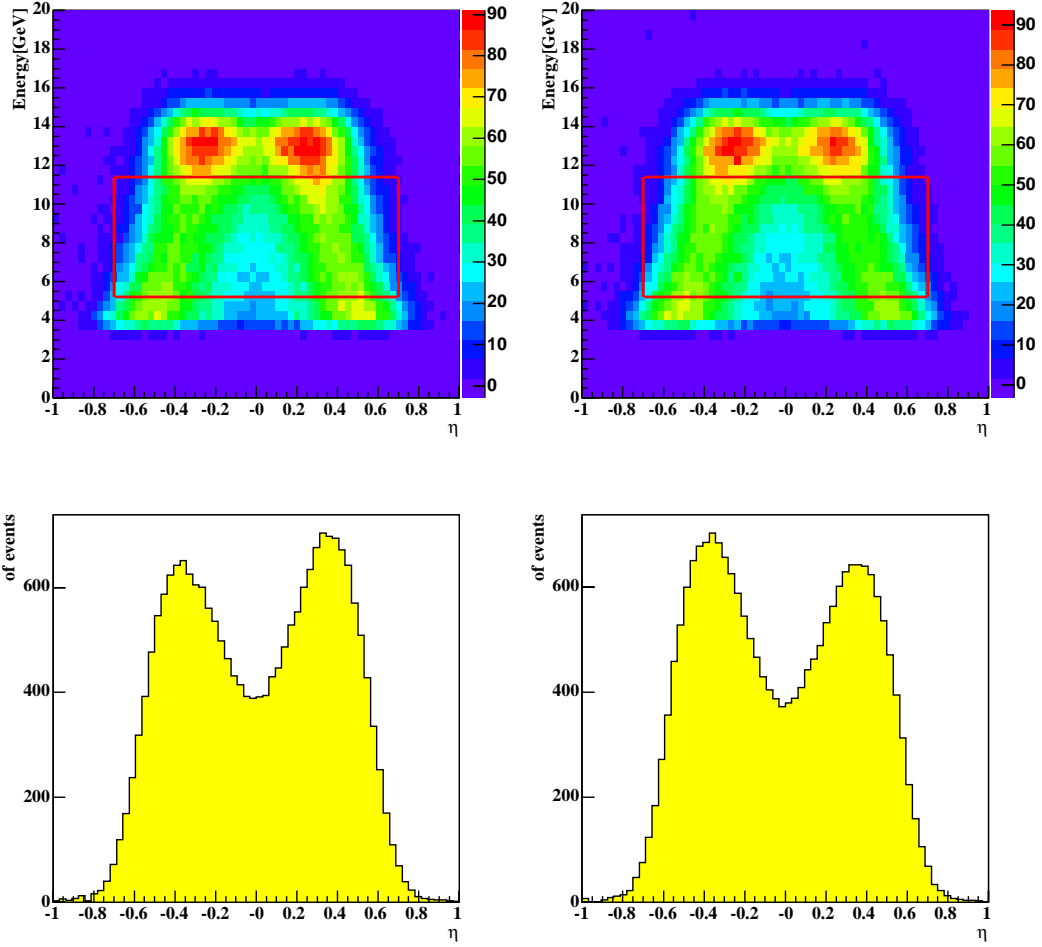


Figure 3.2: Histograms from the data for the averaging method. Upper left and right show two dimensional data from laser-left, laser-right respectively. The used range is indicated by the red box. Lower left and right show histograms projected above the two red boxes to the horizontal axis.

Therefore, the averaging method is not suitable in the situation where these conditions are changeable. Also, the averaging method does not yet fully exploit all sensitivity in the data, in the sense that it takes only average in a limited phase space. For this reason, an alternative analysis method is needed. The alternative method is called “The fitting method” and will be presented in the next chapter.

3.4 Measurement of Longitudinal Polarisation

Σ_{2Z} does not have the azimuthal angle ϕ . Thus, integrating over the vertical position in Eq.(3.24), only Σ_{2Z} is remained. Therefore, the longitudinal polarisation of the lepton beam P_Z is measured from the energy asymmetry of backscattered Compton photons when the laser light is switched its polarity left and right. Then, the function is written as follows:

$$A = \Delta S_3 P_Z \frac{\Sigma_{2Z}}{\Sigma_0}. \quad (3.28)$$

The longitudinal polarisation P_Z can be obtained by fitting the measured energy asymmetry with Eq.(3.28) with $\Delta S_3 P_Z$ as free parameter.

Chapter 4

The Fitting Method

In this chapter, the fitting method[8] will be presented.

4.1 The Fitting Procedure

So far, the response of the calorimeter was not considered but only theoretical approaches were explained. But in practice, the measured energy and the η distributions are convolutions of the cross section and the detector smearing. Therefore, we considered it by a modelling, which describes the calorimeter response function as a Gaussian in the fitting method. Full description is as follows:

- The double differential cross section from laser-left and laser-right in (E_{true}, ϕ) expected theoretically are

$$\frac{d^2\sigma^L}{dE_{true}d\phi} = \Sigma_0(E_{true}) + S_1^L \Sigma_1(E_{true}) \cos 2\phi + S_3^L (P_Y \Sigma_{2Y}(E_{true}) \sin \phi + P_Z \Sigma_{2Z}(E_{true})), \quad (4.1)$$

$$\frac{d^2\sigma^R}{dE_{true}d\phi} = \Sigma_0(E_{true}) + S_1^R \Sigma_1(E_{true}) \cos 2\phi - S_3^R (P_Y \Sigma_{2Y}(E_{true}) \sin \phi + P_Z \Sigma_{2Z}(E_{true})), \quad (4.2)$$

where $S_1^L, S_1^R, S_3^L, S_3^R$ denote the linear and circular component of the

initial photon¹ and P_Y, P_Z denote the transverse and longitudinal components of the initial lepton beam. Also, E_{true} is energy of the backscattered photon².

- At TPOL, ϕ can not be measured, thus we transform ϕ to η using Eq.(3.8) and Eq.(2.5)³. Then, Eq.(4.1) and Eq.(4.2) can be written as follows:

$$\frac{d^2\sigma^s}{dE_{true}d\eta_{true}} = \int \frac{d^2\sigma^s}{dE_{true}d\phi} \frac{1}{\sqrt{2\pi}\sigma_y} \exp\left(-\frac{(y(\eta_{true}) - R(E_{true}) \sin\phi - \delta_y)^2}{2\sigma_y^2}\right) \frac{dy}{d\eta_{true}} d\phi, \quad (4.3)$$

where superscript s means L or R .

- Actually, when ϕ is transformed to η , we considered a part of the calorimeter response : the $\eta - y$ transformation. However, it is not sufficient: the energy and the η response are further considered as follows:

$$\frac{d^2\sigma^s}{dEd\eta} = \int \int \frac{d^2\sigma^s}{dE_{true}d\eta_{true}} \frac{1}{2\pi\sigma_\eta\sigma_E} \exp\left(-\frac{(\eta_{true} - \eta)^2}{2\sigma_\eta^2(\eta_{true}, E_{true})} - \frac{(E_{true} - E)^2}{2\sigma_E^2(E_{true})}\right) d\eta_{true}dE_{true}, \quad (4.4)$$

where $\frac{d^2\sigma^s}{dEd\eta}$ is the expected measured value⁴.

- Using the least squares method, we have to minimise the following function with normalisation k_s, k_{off} :

$$\chi^2 = \sum_{s=L,R} \sum_{E_i} \sum_{\eta_i} \frac{\left(N_{s,i,j}^{on} - (1 - k_{off})N_{s,i,j}^{off} - k_s \frac{d^2\sigma^s}{dEd\eta}\right)^2}{\sigma_{s,i,j}^2}, \quad (4.5)$$

¹L and R mean laser-left and -right, respectively.

²Of course, we can not measure the true energy, so it means an energy distributed in a Gaussian around measured mean energy. Thus, we integrate over the true energy. This applies to η_{true} .

³The $\eta - y$ transformation is included as a calorimeter response function.

⁴ $\sigma_\eta(\eta_{true}, E_{true}) = a\sqrt{\frac{1 - \eta_{true}^2}{E_{true}}}$. See [9]

where $N_{s,i,j}^{on}$ and $N_{s,i,j}^{off}$ are laser-on data and laser-off data, respectively. E_i and η_j are the energy and the η of bin (i, j) ⁵.

In the next section, we will describe all the parameters in detail.

4.2 The Fitting Parameters

There are two categories of the fitting parameters. Some of the fitting parameters are made such that they are sensitive to the polarisation helicity data, i.e. laser-left and laser-right.

- Normalisation
 - N^L, N^R : the overall normalisation.
These parameters are described as k_s in Eq.(4.5).
- Laser
 - S_1^L, S_1^R : the liner laser polarisation.
- Polarisation
 - $S_3^L \cdot P_Y, S_3^R \cdot P_Y$: the transverse lepton beam polarisation.
 - $S_3^L \cdot P_Z, S_3^R \cdot P_Z$: the longitudinal lepton beam polarisation.

These 6 polarisation parameters(laser and lepton beam) are included in Eq.(4.1) and Eq.(4.2).

All the other fitting parameters are common for both helicity states;

- Lepton beam
 - σ_y : the transverse width of lepton beam at the IP, called the beam size.
 - δ_y : the vertical offset between the centre of lepton beam and the centre of the calorimeter,

where σ_y is used as a sigma in smearing y position with a Gaussian in Eq.(4.3), then δ_y corresponds to the offset.

⁵In the fitting method, two dimensional data of (E, η) are divided by 64 in E and 128 in η .

- The calorimeter:

following parameters are considered in the calorimeter response.

- $P1, P2, P3, P4$: the η - y transformation parameters. The formula is defined in Eq.(2.5).

- a, b : the energy resolution.

$$\frac{\sigma_E}{E} = \frac{a}{\sqrt{E}} \oplus b, \quad (4.6)$$

where a is the stochastic term and b is the constant term and \oplus means quadratic sum.

The σ_E in Eq.(4.6) is used as a sigma in smearing energy with a Gaussian and the stochastic term a is used in σ_η in Eq.(4.4).

- f_e and f_η : these parameters are calibration factors for the energy and the η scale and reflect an imperfect calibration of the calorimeter up and down sides, then parametrised as:

$$E_{obs} = f_e \times E_{calo} \times (1 + f_\eta \times \eta_{calo}), \quad (4.7)$$

$$\eta_{obs} = \frac{\eta_{calo} + f_\eta}{1 + f_\eta \times \eta_{calo}}, \quad (4.8)$$

where E_{obs} and η_{obs} mean the read out quantities. E_{calo} and η_{calo} mean what is expected quantities in the calorimeter after smearing with a Gaussian. Then, it can be rewritten as follows for the up and down sides:

$$U_{obs} = (f_e \times (1 + f_\eta)) \times U_{calo}, \quad (4.9)$$

$$D_{obs} = (f_e \times (1 - f_\eta)) \times D_{calo}, \quad (4.10)$$

where U_{obs} , D_{obs} , U_{calo} and D_{calo} are the energy defined in Eq.(4.7) for up and down sides. Therefore, the imperfect calibration effect can be expressed by these factors for the up and down sides, i.e. as expected from imperfect voltages settings of PMTs.

- $d0$: distance between the IP and the calorimeter surface. If the lepton beam change its orbit due to some effects⁶, the laser light is adjusted,

⁶Also discussed in section 5.2.

so that the laser light and the lepton beam can collide properly. Thus, this distance can be changeable.

4.3 Background Subtraction

At first, the bremsstrahlung background is removed by subtracting laser-off data from laser-on data before fitting, because the laser-on data includes the signal and the background, and the laser-off data includes the background only. Then the laser-on data and the laser-off data are normalised by the shutter opening and closing time, respectively. Also this background subtraction is made for laser-left and laser-right, separately. Finally, the fit to the double differential cross section for Compton scattering is done and this fit is made for every one-minute intervals of the measurement cycle.

4.4 Determination of parameter set

In this section, studies for determining the parameters set for the fitting method will be presented, so that we can decide which parameters should be free and which parameters should be fixed. For that, we checked the fit stability and compared with the data and the results of fit.

4.4.1 Stability against η range

This fitting method is based on the idea that all information related to the lepton beam, the laser light and the calorimeter are introduced in the fit as a free parameter, so that these information can be determined. However, this idea may be ideal thus we need to study to see if the fitting method work. In this method, we can change the number of data used for the fitting by changing η range.

First of all, we checked the stability of the method against the fitting range in η . If the fitting method worked fine, fitting parameters should be stable against the fitting range in η . There exists many parameters in the fitting method and it is needed to check which parameters should be free, which parameters should be fixed such that this fitting method works fine. We suspected that results of the fitting may fluctuate by changing the amount of data used for the fitting, thus we ran the method by changing the η range

from between ± 0.1 to ± 0.8 with 0.1 interval for checking the stability of some parameters against η range.

At first, the fitting was examined with all parameters free except that $S_3^L \cdot P_Z, S_3^R \cdot P_Z$ were fixed to be 0. Figure 4.1 shows the results. In these plot, a transverse polarisation value from the fitting method is symbolised as to TPOL and a longitudinal polarisation value from other independent analysis is symbolised as to LPOL, and the LPOL/TPOL ratios were checked. Because the LPOL is an independent detector from the TPOL, it is possible to use as a good reference. Also, Beamsize, $\Delta S1$, Resolution, yoff and Distance mean $\sigma_y, S_1^L - S_1^R, a, \delta_y$ and $d0$, respectively.

In those plots, Distance is unstable in η especially and it means that the method does not have good stability yet. Then, η - y curves were compared between the one extracted from this method and the other from the measurement with the silicon detector. Figure 4.2 shows these two curves. Comparing two η - y curves, there is a large difference between them. It indicates that the fitting method can not reproduce the data under this parameter condition. Therefore, we decided to fix the η - y parameters at the values obtained by the measurement with the silicon detector.

Then, the stability against η range was examined again with the η - y parameters fixed. Figure 4.3 shows the results. Actually, parameters of the η - y curve were extracted from real measurement, but fitting parameters were not stable against fitting range, especially Resolution and Distance were unstable. Therefore, these two parameters also have to be fixed. In 2001, TPOL test beam measurements have been done at CERN [10], then the energy resolution has been measured. Thus, this parameter will be fixed to the test beam value and Distance will be fixed to be 65m.

Next, the stability was checked again with Resolution and Distance fixed. Figure 4.4 shows the results. With these two parameters being fixed, other fitting parameters were almost stable against η ⁷. Therefore, it can be concluded that this fitting method works anyway.

4.4.2 Determination of the fitting range

What should be done next is to decide which η range is most suitable for the fitting range. For that, we compared the LPOL/TPOL ratio using the

⁷Acually, LPOL/TPOL and Beamsize are unstable in low η range. But, it is due to small amount of the data. Thus, it should not consider the unstable in the range.

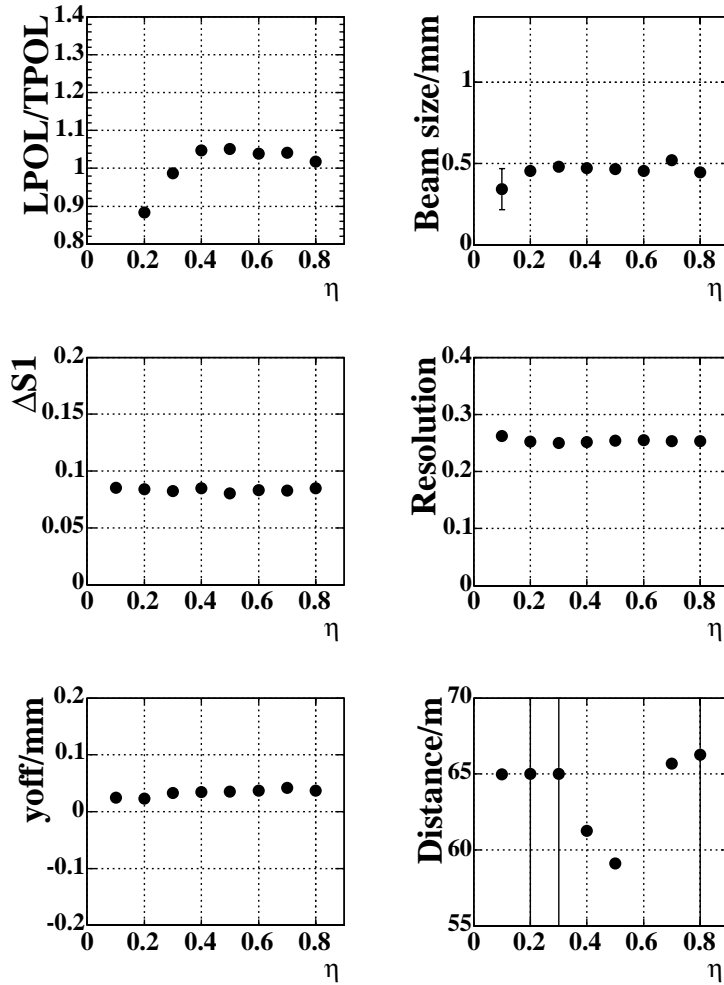


Figure 4.1: Fitting parameters as a function of the η range. For example, η is 0.5 means that data between ± 0.5 is used for the fitting

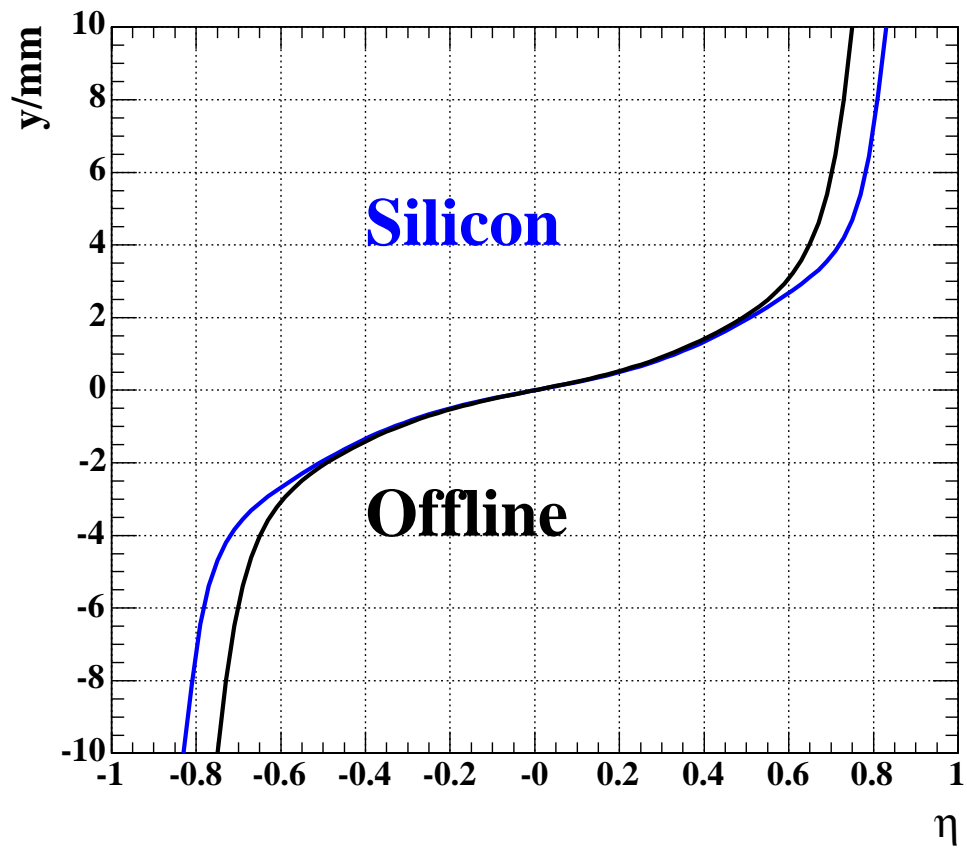


Figure 4.2: The blue line is created with parameters extracted from the silicon detector. The black line is the one with parameters extracted from the fitting results.

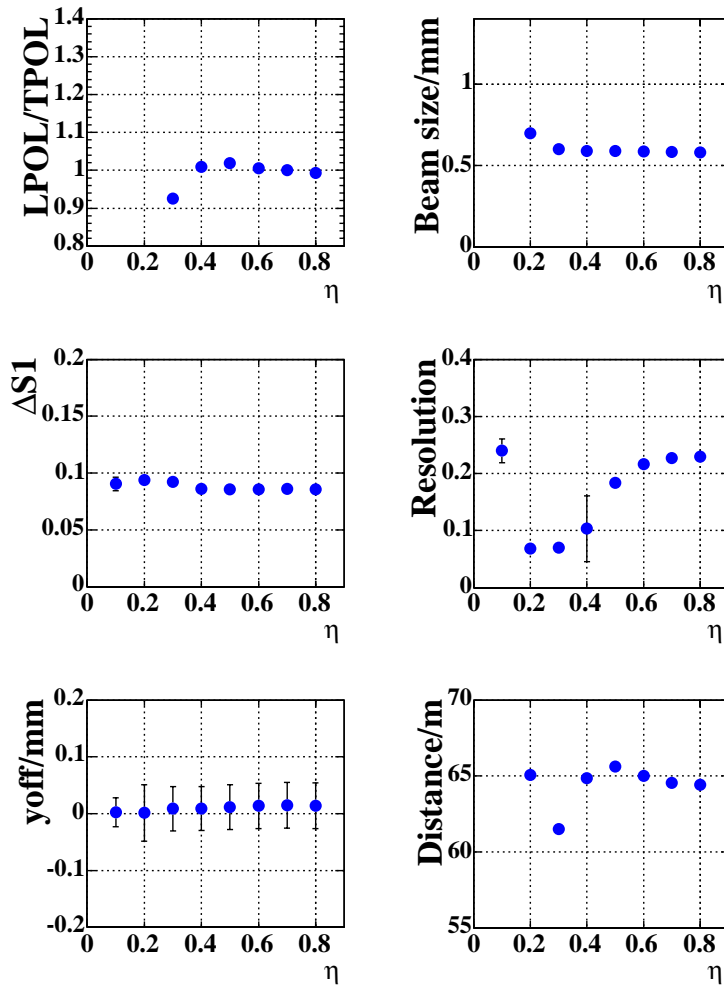


Figure 4.3: Fitting parameters as a function of the η range. For example, η is 0.5 means that data between ± 0.5 is used for the fitting

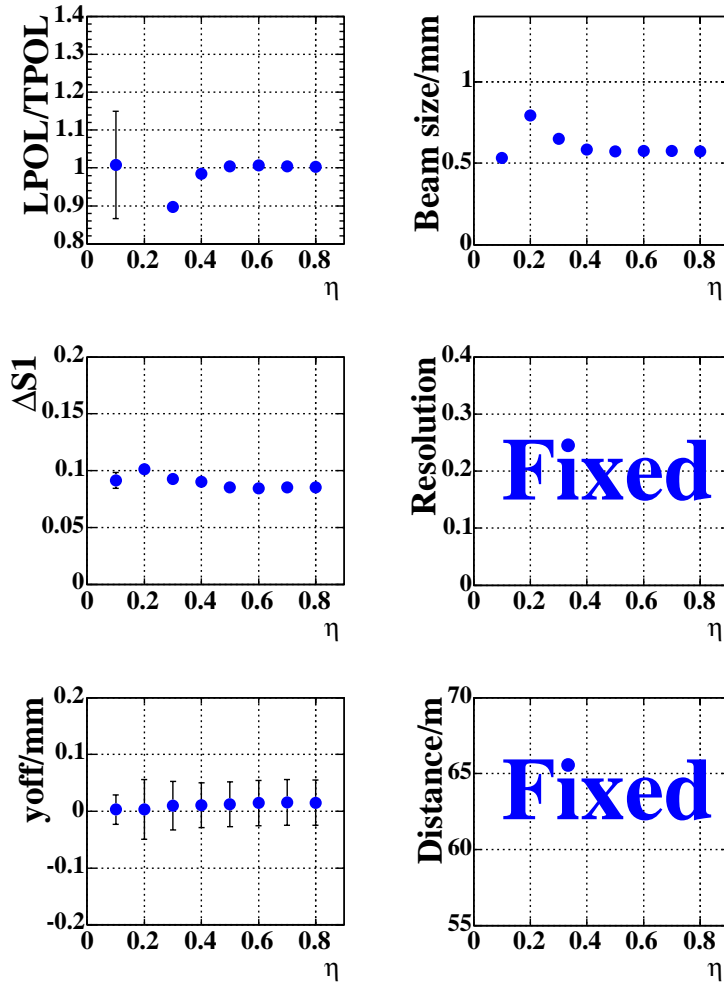


Figure 4.4: Fitting parameters as a function of the η range. Some fitting parameters against η range. Now, the energy resolution and the distance are fixed. For example, η is 0.5 means that data between ± 0.5 is used for the fitting

η - y curve from the Normal mode with the one from the Table scan mode⁸. Looking at Figure 4.5, η range from ± 0.4 to ± 0.6 seems to be good as a fitting range, because the fitting parameters are almost stable in this region. According to this study, the region less than ± 0.4 and greater than ± 0.6 are excluded. The reason is as follows:

- In high η region, backscattered particles from the calorimeter and the particles entering with some angle due to the pre-radiator seems to be dominant. Therefore, there seems to have bias in deriving the η - y curve.
- In low η region, those fitting parameters are not stable against η range.

Therefore, it is reasonable that the region between ± 0.5 is selected for the fitting range.

4.4.3 Comparison between Data and Fit

To investigate further, the bin-by-bin wise comparison between the data and the fitting results were performed by using pull, where pull is defined as:

$$\mathbf{Pull} \equiv \frac{(\mathbf{Data} - \mathbf{Fit})}{\delta\mathbf{Data}}. \quad (4.11)$$

In Figure 4.6 shows histograms and pulls stored for 1 minute data taking cycle with laser-left and -right, respectively. Actually, parameters were almost stable against the fitting range in previous stability check but looking at the pull in Figure 4.6, the difference between the data and the fit results seems to be large at laser-left and -right, respectively. The polarisation, however, can be calculated with the histogram subtracting laser-right from laser-left in the end⁹. Therefore, judging from the subtracted pull, it can be concluded that this fitting can almost reproduce data and work fine.

Also, looking at pulls of each laser state, there are some asymmetric shapes in η . These asymmetric shapes will be discussed later in chapter 7.

⁸This check is to minimise the systematic uncertainty from the difference of the η - y curve.

⁹As described in section 3.2, the polarisation can be calculated from the asymmetry and this asymmetry can be maximum when laser-right is subtracted from laser-left.

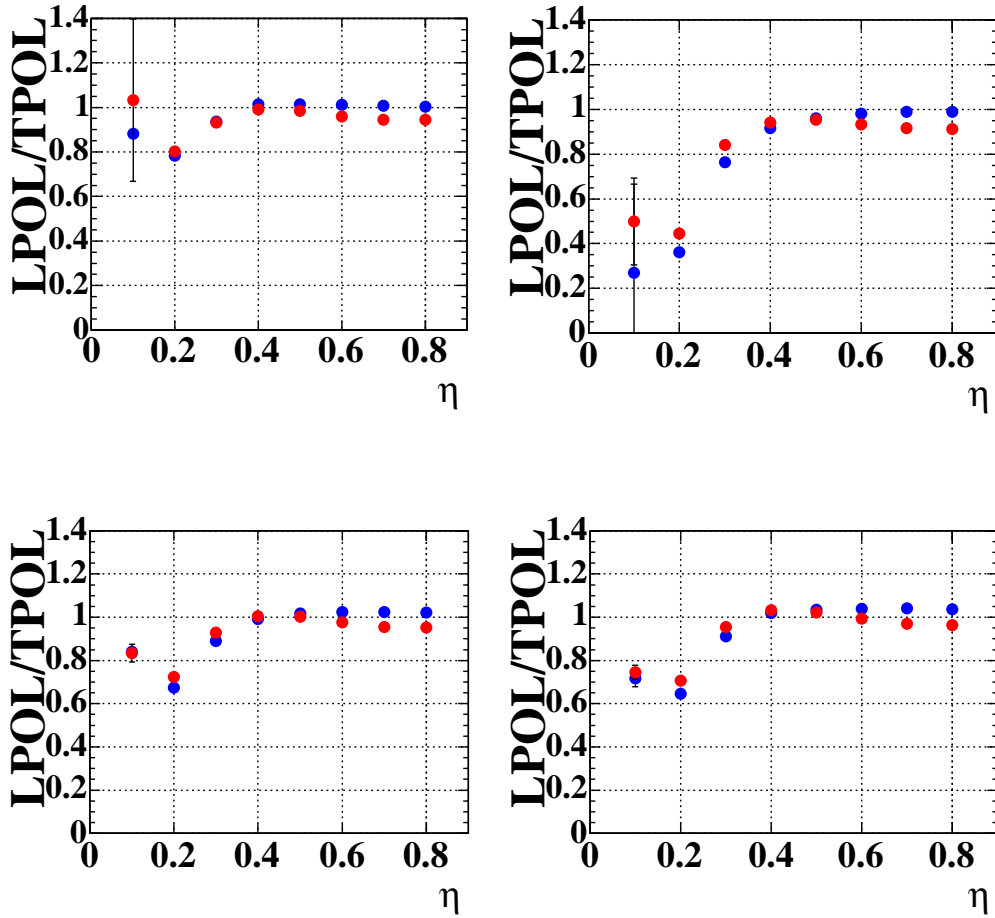


Figure 4.5: The LPOL/TPOL ratios as a function of the η range for four data sets. Red dots and bars are from the Table scan mode and blue dots and bars are from the Normal mode. For example, η is 0.5 means that data between ± 0.5 is used for the fitting

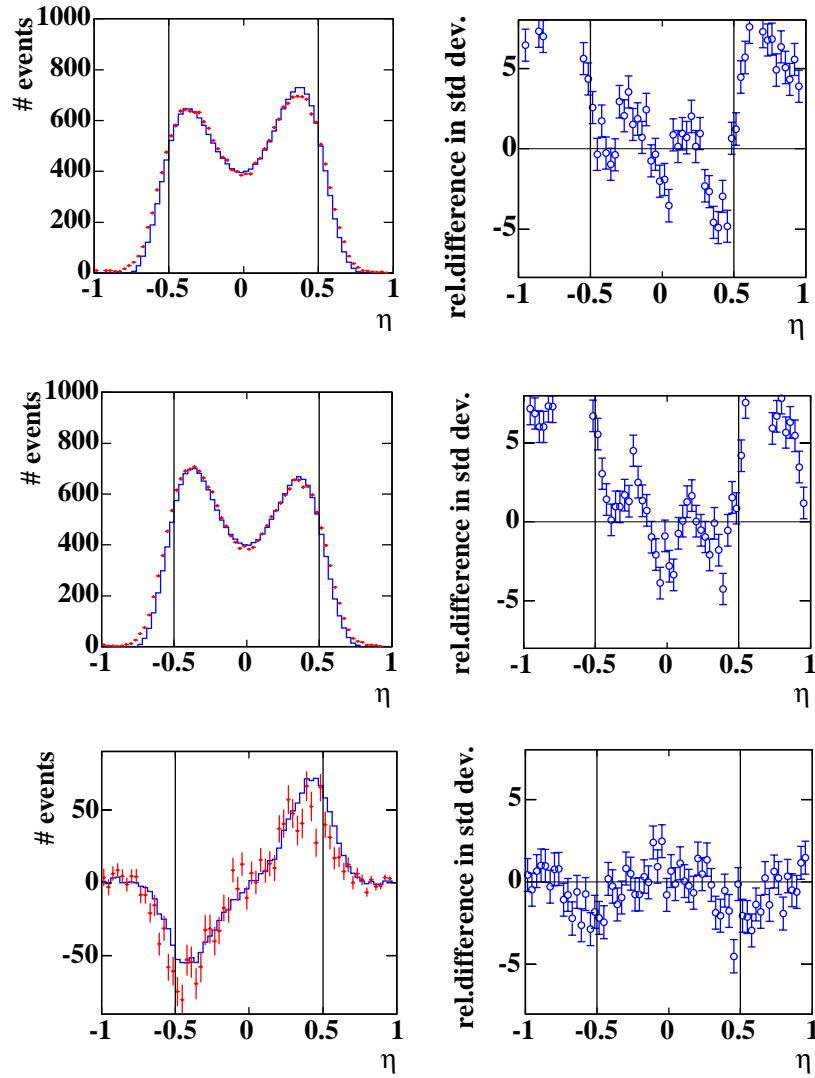


Figure 4.6: Histograms and binwise pulls from the data and the fitting. Left column from top to bottom shows histograms with laser-left, laser-right and the one subtracting laser-right from laser-left, respectively. Red dots and error bars indicate the data, blue histograms show the final results of the fitting and black lines indicate the fitting range. The plots in the right column show the binwise pulls calculated using the same data indicated in the histograms shown in the corresponding left column. The energy range is between $5.2 \text{ GeV} < E_\gamma < 11.4 \text{ GeV}$. This range is same as the averaging method and is most sensitive region to the polarisation.

Finally, the final parameters set are determined and their status are shown in Table 4.1. Then we will analysed all polarisation data under this parameters condition. Those results will be presented in the next chapter.

Parameters	status
η - y 4 parameters	the Normal mode
η range	between ± 0.5
σ_y	free
δ_y	free
$d0$	fixed to 65m
f_e, f_η	free
a	fixed to the beam test value
b	free

Table 4.1: Fitting parameters

Chapter 5

Systematic Errors

5.1 Overview

We considered the following systematic error sources:

- the beam related
 - uncertainty in $d0$.
 - δy .
- the calorimeter related
 - choice of the η -y curve.
 - change of the fitting range.
 - calibration of the calorimeter.
 - energy resolution of the calorimeter.

These items are discussed and estimated in the following sections.

5.2 Distance from the IP to the calorimeter

The possible reason that the distance can be changeable is as follows[11]:

- Laser and the lepton beam can be changeable their condition then the alignment of the laser beam is sometimes adjusted to collide the lepton beam properly, so that the IP position could change.

- The position and the direction of the lepton beam would change the IP.

Due to these effects, the distance would change. Thus, by an educational guess, the systematic error from this source was estimated by changing the distance by $\pm 1\text{m}$ from 65m .

5.3 Vertical beam offset

The backscattered Compton beam has symmetric distribution along vertical direction of the calorimeter in averaging laser-left and laser-right. Thus, it is expected that the centre of the calorimeter and the averaged hit position of the incident particles on the calorimeter should match ideally. In the fitting method, we considered δ_y as a free parameter. It indicates that the fitting method can determine the offset. We checked to see if this consideration was reasonable. For that, we assumed that the TPOL was perfect aligned to the backscattered Compton beam, so that the centre of the beam matched to the centre of the calorimeter. Thus, we estimated systematic error from this source with the δ_y fixed to 0.

5.4 Choice of the η - y curve

One of the major systematic errors seems to arise from the uncertainty of the precision of the η - y curves as described in section 3.3. Considering the beam profile, there clearly exists the difference between the the Table scan mode and the Normal mode (See Figure 5.1). Therefore, the difference of the profile probably causes the maximum difference in deriving the η - y curve and we take data in Table scan mode to estimate the systematic error due to the difference between the Normal mode and the Table scan mode.

5.5 Change of the fitting range

We can change the fitting range in the fitting method, so that we can check how impact on the results by changing the amount of data used for the fitting since it is expected that the results of the fitting should not depend on the amount of the data used to the fitting. As described before, between the

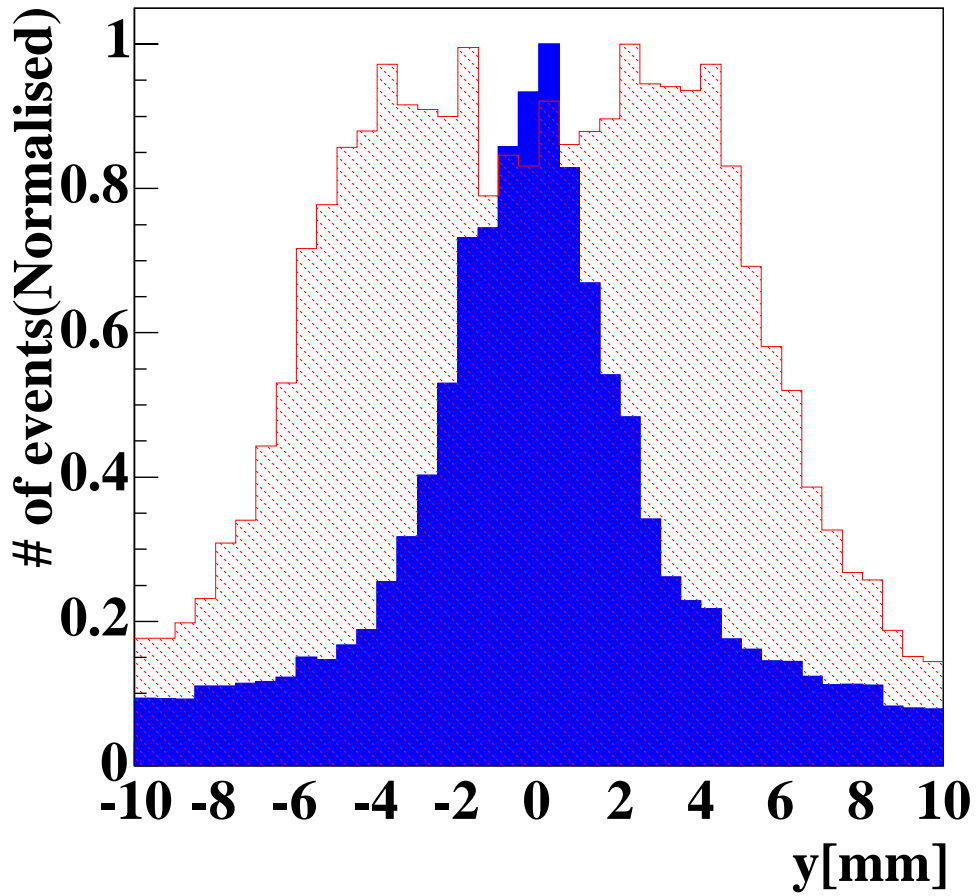


Figure 5.1: Beam profile from the Table scan mode and the Normal mode. Red histogram is from the Table scan mode and blue histogram is from the Normal mode.

range ± 0.5 in η is used for fitting range as a nominal. We estimated the systematic error from the amount of data used for the fitting by changing the fitting range ± 0.05 in η around the nominal.

5.6 Calibration of the calorimeter

In Eqs.(4.7),(4.8), there are two parameters, f_e and f_η which reflect the imperfect calibration of the calorimeter. If the calorimeter is always calibrated perfectly, $f_e = 1$ and $f_\eta = 0$. Actually, we do not understand how much the imperfectness of the calibration at present. Therefore, the systematic error from this source was estimated by being constrained these two parameters to above values though it is probably overestimation.

5.7 Energy resolution of the calorimeter

According to the test beam at CERN, the energy resolution was evaluated to 23.77% at the beam energy from 6 GeV to 40 GeV. On the other hand, the energy resolution can be also obtained from a direct fitting to the Compton edge *in-situ*. Figure 5.2 shows the background subtracted energy distributions and the fitting curve to the derivatives of the Compton edge.

The way to estimate the energy resolution from Compton edge is as follows [12]:

- Plot background subtracted energy distributions.
- Plot derivative of Compton edge.
- Fit to the derivative distributions with Gaussian and extract σ .
- Repeat same procedure for different data sets.

Table 5.1 shows the energy resolution calculated from above procedure. Averaging those values, the energy resolution was $0.739 \pm 0.001[\text{GeV}]$. This value corresponds to 19.68% for the stochastic term. Therefore, the fitting ran with fixing the stochastic term as 19.68% for estimating systematic error from the energy resolution.

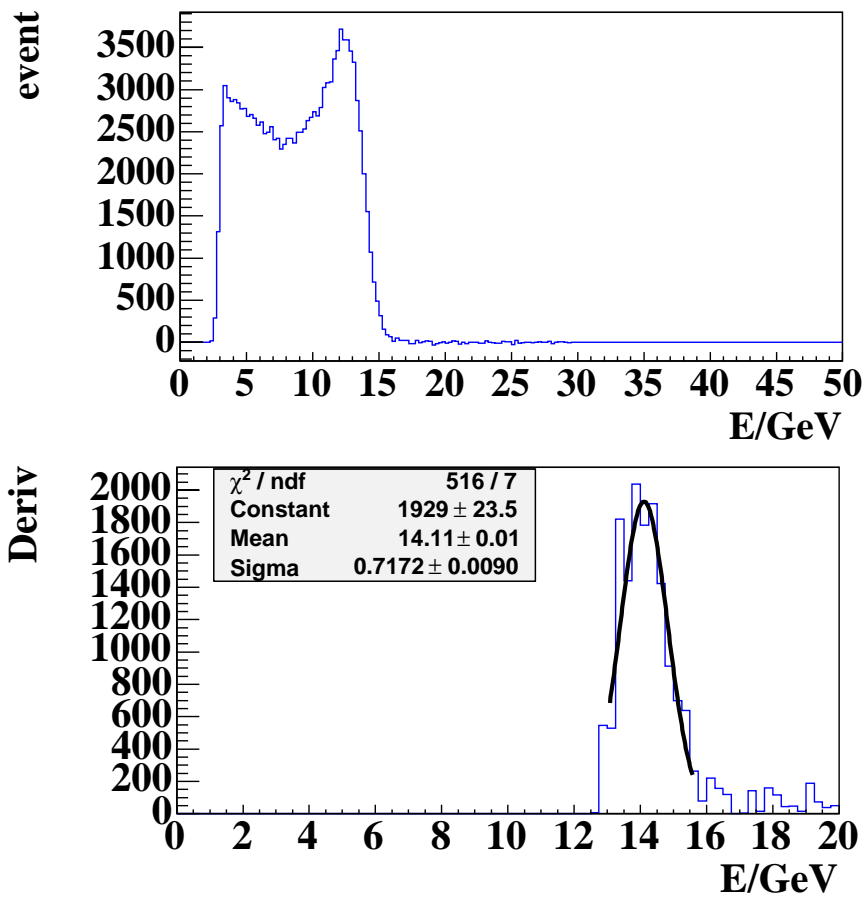


Figure 5.2: Upper plot shows the energy deposited in the calorimeter and the lower plot shows the derivative of Compton edge.

Date	σ/GeV
31st.Jan	0.717 ± 0.010
25th.Feb	0.859 ± 0.011
1st.Mar	0.722 ± 0.003
7th.Mar	0.727 ± 0.001
24th.May	0.748 ± 0.002
11th.Aug	0.695 ± 0.002

Table 5.1: The energy resolution from Compton edge [12].

5.8 Summary of systematic checks

The total systematic error from several sources listed above was evaluated as a quadratic sum as:

$$\delta(syst) \equiv \sqrt{\sum_{i=source} (\delta^i(syst)^2)}. \quad (5.1)$$

Table 5.2 shows systematic errors from several sources and total systematic

Source	Error[%]
Distance	-0.78
Beam offset	0.02
The η - y curve	-0.87
Fitting range	-1.99
Calibration	1.97
Resolution	1.16
Total	3.248

Table 5.2: Systematic errors from various sources.

error is 3.248% mainly due to the fitting range and the calibration of the calorimeter. However, it is found that some asymmetric structures exist in the binwise pulls as described in the previous chapter. Therefore, there may exist other systematic errors except for mentioned above. This will be described and discussed in the next chapter.

Chapter 6

Results and Discussion

We have analysed all data from October 2003 to August 2004 with the fitting method. In this chapter, we will present results and discuss their adequacy.

6.1 Comparison with the LPOL

At first, we compared the results of the fitting method with the LPOL. Figure 6.1 displays the LPOL and the TPOL for one HERA beam fill. Comparing with the results from the averaging method, it is seen that the difference between the LPOL and the TPOL become small and it means that the polarisation values are improved with the fitting method. For all data, we also compared with the LPOL and the TPOL with the fitting method. Figure 6.2 displays the comparison and it is seen that the TPOL and the LPOL agree with each other throughout all data.

Next, to check further we compared the LPOL/TPOL ratios calculated from the averaging method with the ones from the fitting method. As described before, the ratio have been off by 10% from 1 and it has been the most serious problem for a long time. Figure 6.3 shows the results. Comparing with the results from the averaging method, σ of the LPOL/TPOL ratios calculated from the fitting method is getting smaller with more averaging time. Also, there is no strange dip in the histograms with more averaging time which is clearly seen in the ones from the averaging method and the χ^2 /Number of degrees of freedom (ndf) are shown in Figure 6.4. Actually, the polarisation can be calculated minute by minute both the averaging method and the fitting method. Thus an entry in the histograms is the calculated

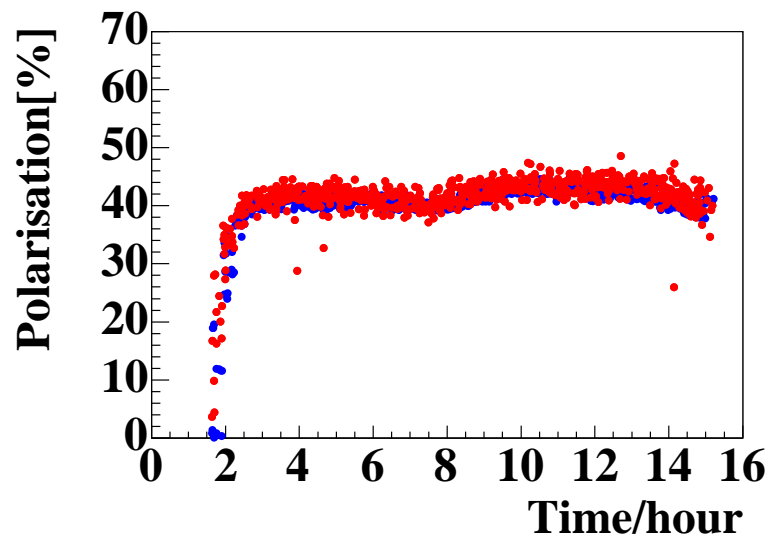
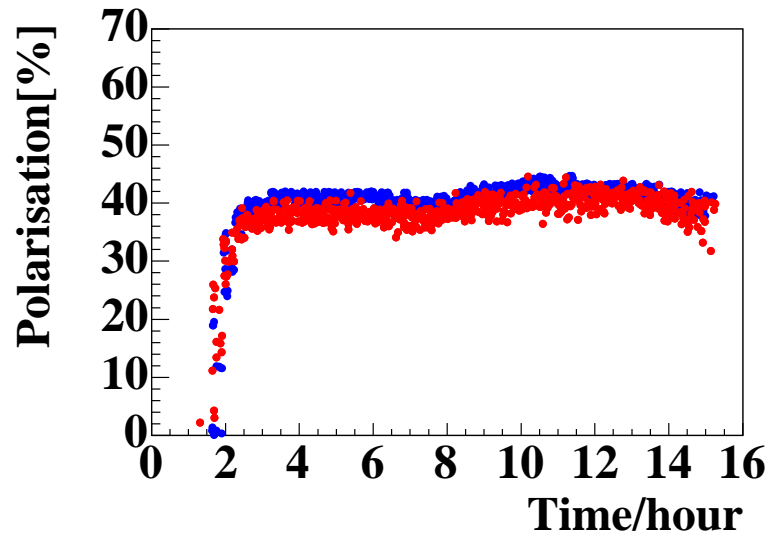


Figure 6.1: Comparison between the LPOL and the TPOL for 1 beam fill. Blue dots are the LPOL and the red dots are the TPOL. Upper plot shows the LPOL and the TPOL with the averaging method and the lower is the LPOL and the TPOL with the fitting method.

value in 1 minute. Here, 10 minutes average means the averaged polarisation value in 10 minutes with the 1 minute averaged values not averaging in 10 minutes for calculating the polarisation,¹ so that systematic errors are more dominant than statistical errors with more averaging time. Figure 6.3 and Figure 6.4 indicate that the model used for describing the calorimeter in the fitting method is suitable for the polarisation analysis and the fitting works fine². From these plots, it can be concluded that the results of the averaging method include some systematic uncertainties, so that the difference between the LPOL and the TPOL has been around 10% due to the unsuitable modelling.

6.2 Focus Correction

As described in chapter 3.3, the averaging method has disadvantage in the situation where the beam condition can be changeable. According to some investigations, it has been found out that the averaging method has strong dependence on the focus size. The focus size is calculated as follows:

- use data in the energy range $11.2 \text{ GeV} < E_\gamma < 13.8 \text{ GeV}$,
- create one dimensional histograms in η with $-0.890625 < \eta < 0.890625$,³
- subtract the laser-off data from the laser-on data,
- calculate RMS² of the laser-left and the laser-right histograms and the mean η of the those histograms.

Then,

$$\eta = \frac{1}{2}(\bar{\eta}_L + \bar{\eta}_R), \quad (6.1)$$

$$\Delta\eta = \sqrt{\text{RMS}_L^2 + \text{RMS}_R^2}, \quad (6.2)$$

$$\text{focus} = \frac{dy(\eta)}{d\eta} \Delta\eta, \quad (6.3)$$

¹100 minutes average is same as well.

²If the modelling is wrong, there must exists strange dips in the histograms like the averaging method.

³Compton photons within the region of energy and η are almost insensitive to the polarisation, so that the focus size can be calculated.

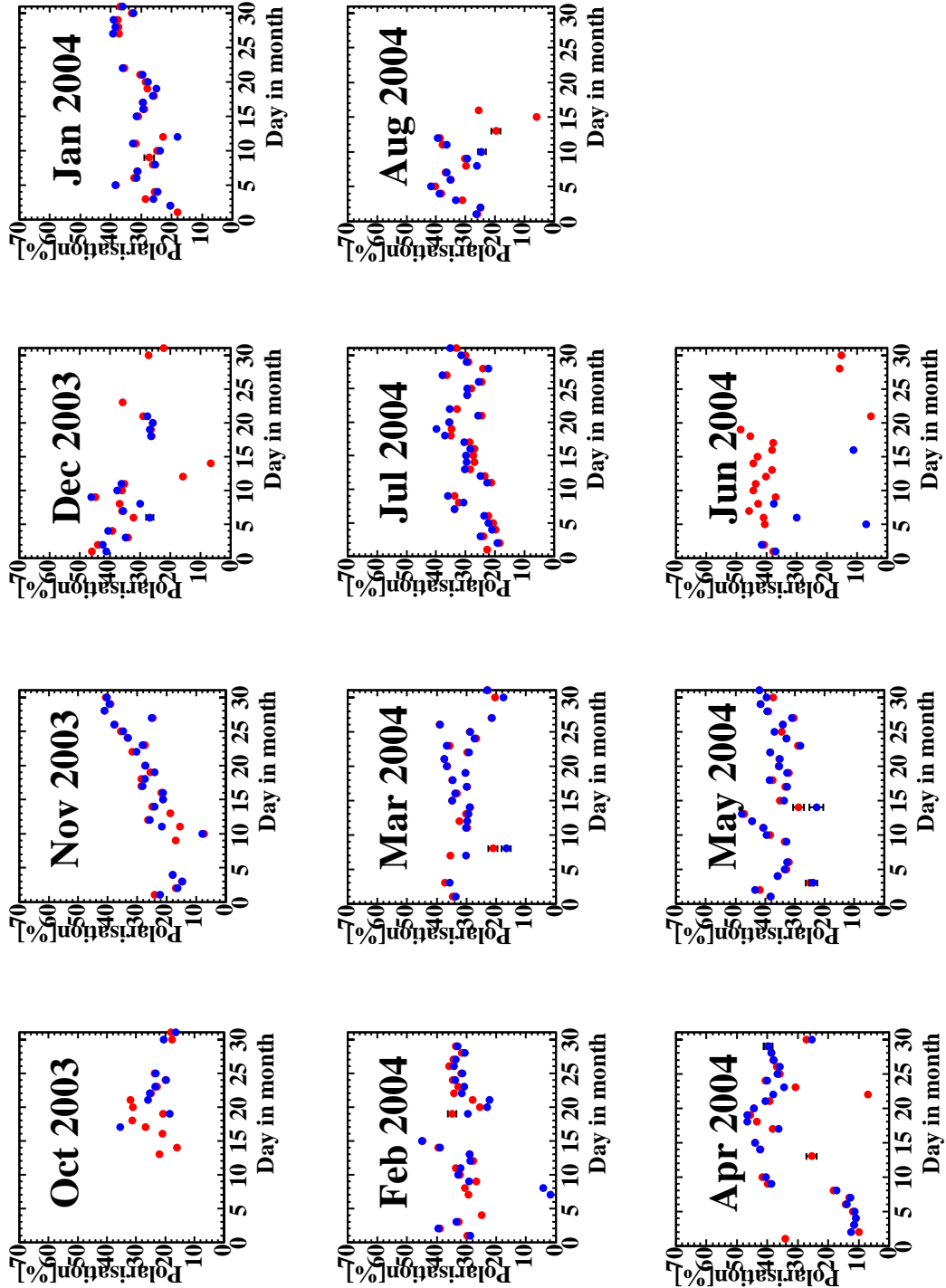


Figure 6.2: Day by day comparison between the LPOL and the TPOL. Left and middle 8 plots are from right-handed positron and right 4 plots are from left-handed positron. Blue points are polarisation measured on the LPOL and red points are the fitting results of the TPOL.

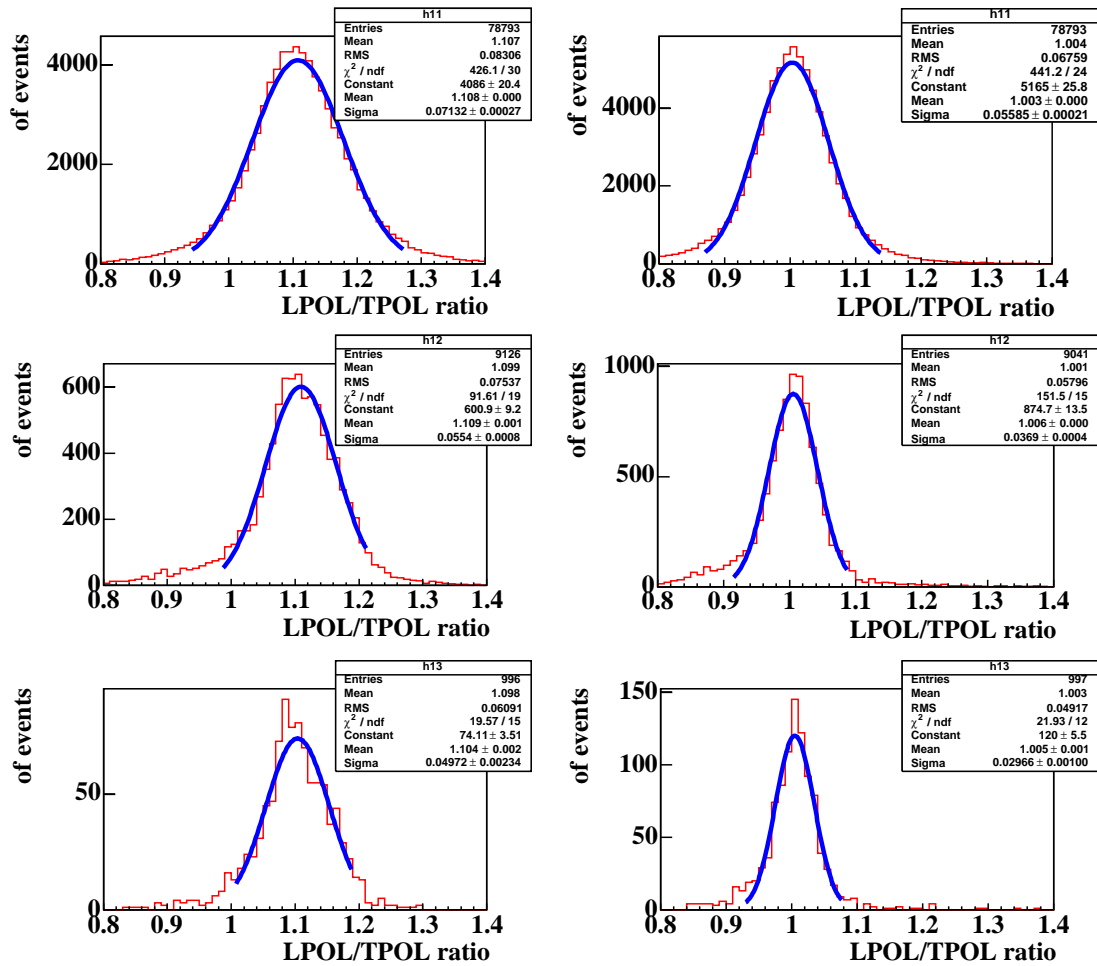


Figure 6.3: Comparison between the averaging method and the fitting method about the LPOL/TPOL ratio. Left columns denote the ratio with the averaging method and right columns are with the fitting method. Upper plots are results with 1 minute average, middle plots are 10 minutes average and lower plots are 100 minutes average.

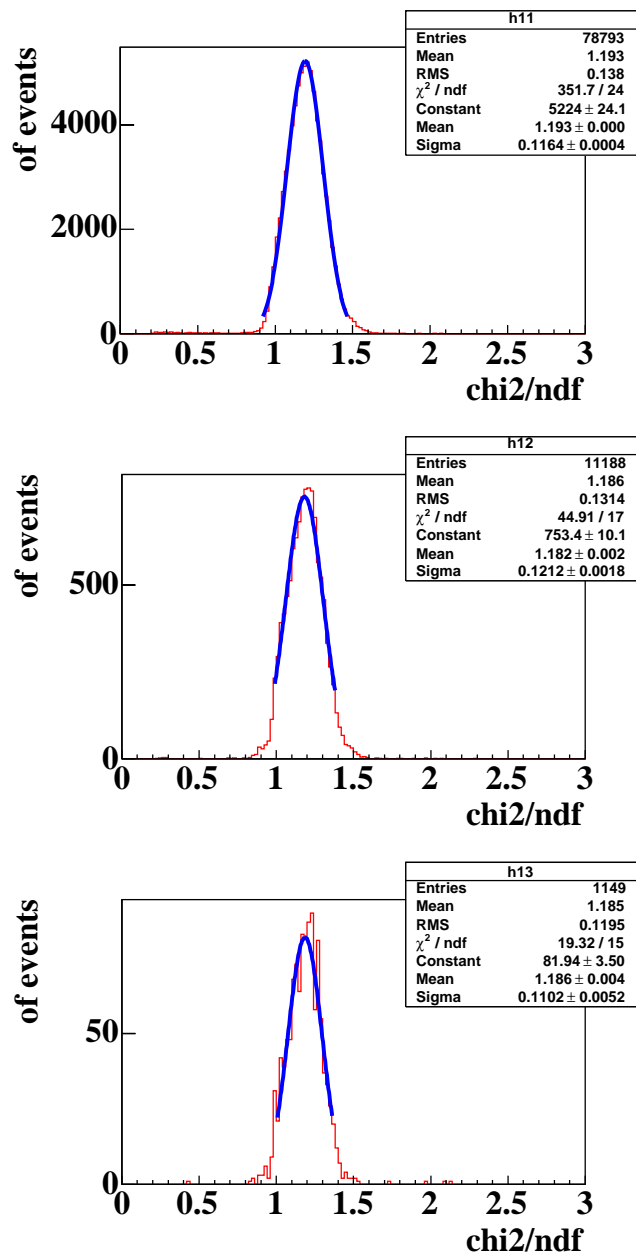


Figure 6.4: The χ^2/ndf . From top to down, the averaging time is 1 minute, 10 minutes and 100 minutes.

where $\bar{\eta}$ means averaged value in η and the subscript L, R mean the laser-left and laser-right, respectively.

Due to this strong dependence to the focus size, the difference between the LPOL and the TPOL has been around 10% with the analysis using the averaging method.

At present, a correction function for the focus dependence was estimated by MC and applied to the averaging method[13]. As a result, the LPOL and the TPOL agree with each other within 2%. Although there is no focus size parameter in the fitting method, there is the beam size parameter instead of it. Actually, correlation between the focus size and the beam size is seen clearly, so that it is possible to check if the focus dependence can be absorbed in the fitting method. Figure 6.5 and Figure 6.6 show the correlation and the focus dependence.

Looking at the Figure 6.6, it is clearly found that there is the focus dependence of the LPOL/TPOL ratio in the analysis using the averaging method. On the other hand, the fitting method can almost absorb the dependence. Also, Figure 6.7 displays the focus correction function estimated by MC and by the fitting method.

function	slope	offset
MC	0.6649	0.7009
the fitting method	0.6658 ± 0.1816	0.7236 ± 0.1052

Table 6.1: Slope and offset of the focus correction function

The slope and offset of the function are shown in the Table 6.1. Looking at the slope, it is clear that the fitting method can reproduce the focus correction function used in the averaging method.

6.3 Vertical beam offset

We considered the vertical offset between the centre of backscattered Compton beam and the centre of the calorimeter as a free parameter, δ_y , in the fitting method. Here, we checked the behaviour of the parameter. Figure 6.8 shows the day by day plot of δ_y throughout all data and Figure 6.9 shows the dependence of the LPOL/TPOL ratio against δ_y . Considering the beam

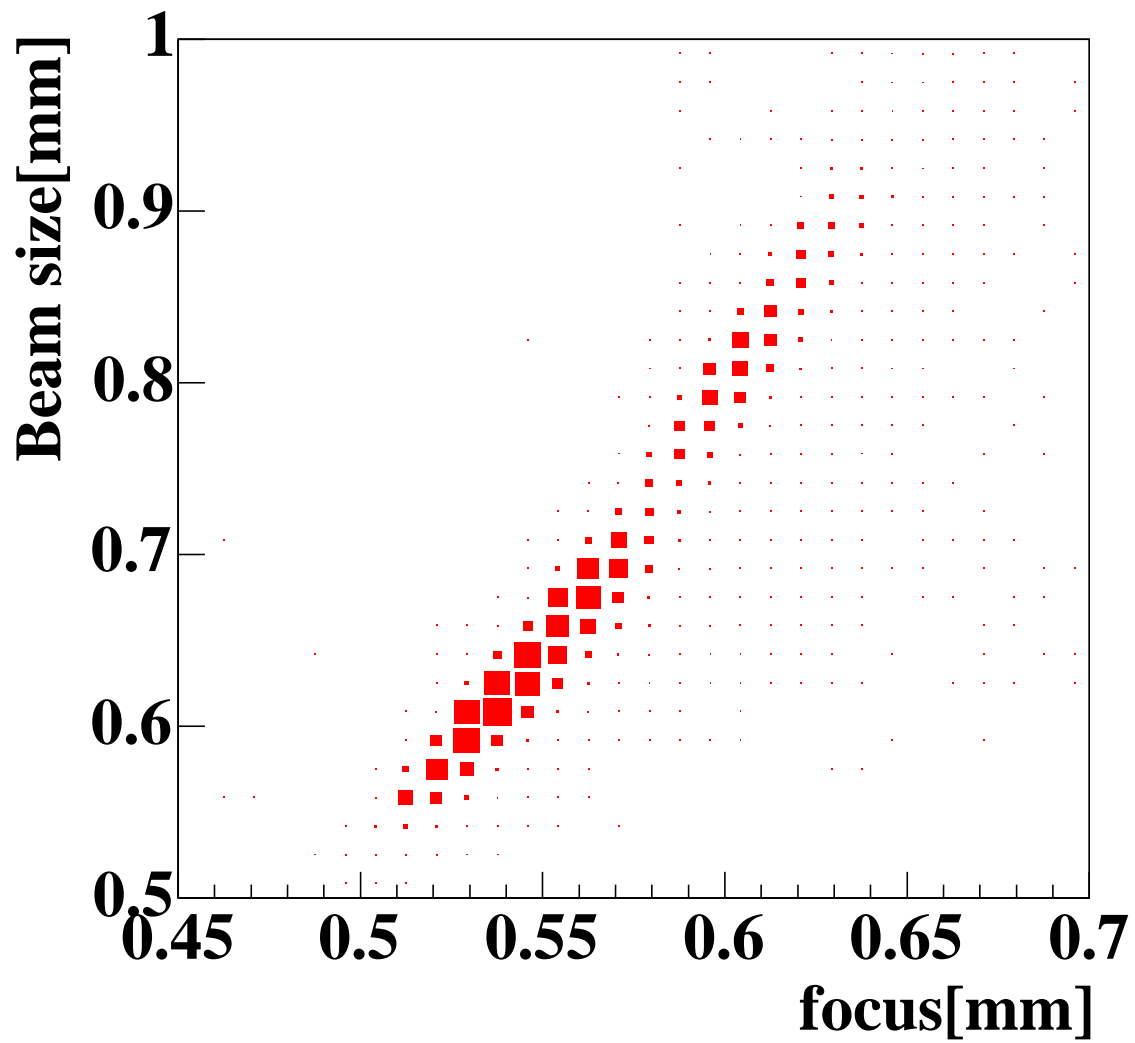


Figure 6.5: Correlation between the focus size and the beam size

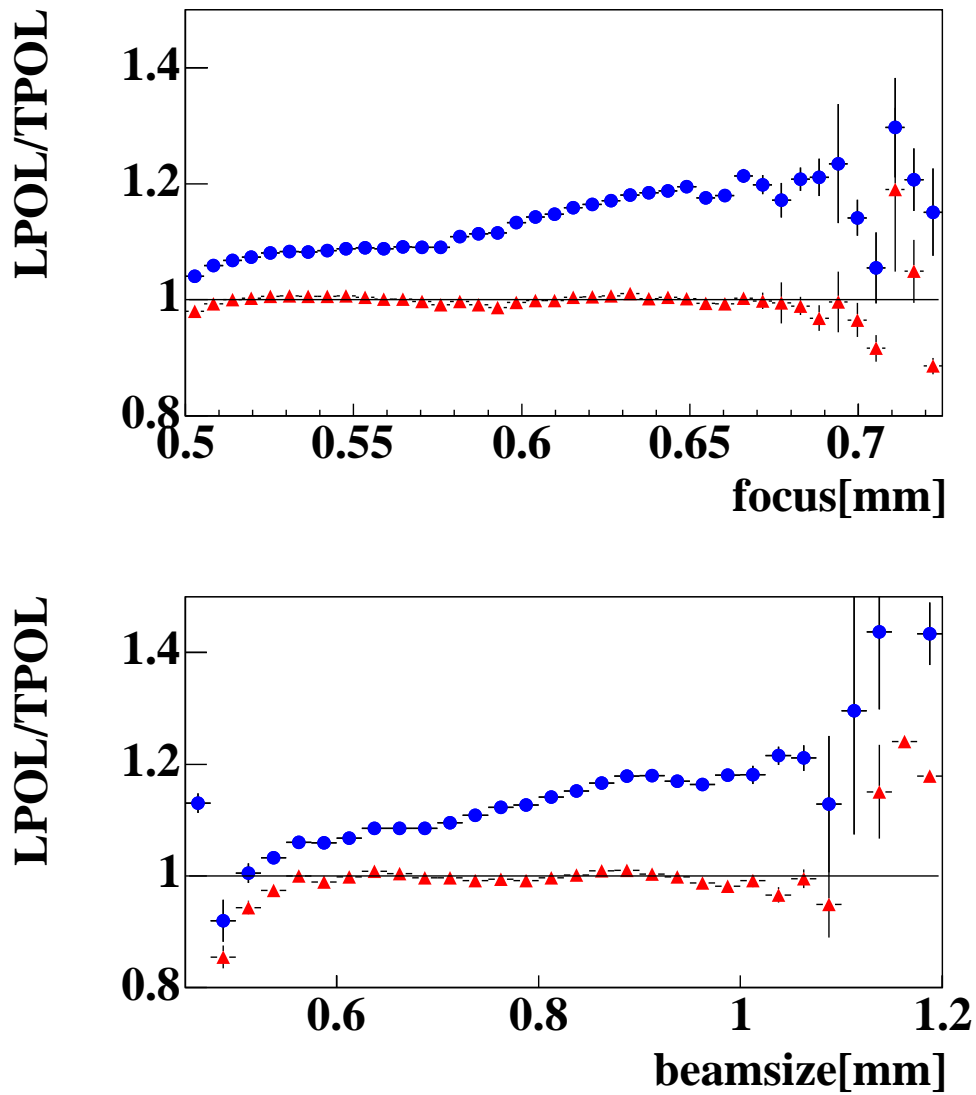


Figure 6.6: Upper plot indicates a dependence of the LPOL/TPOL ratio against the focus size and the lower indicates the one against the beam size. Blue points are from the averaging method and the red ones are from the fitting method.

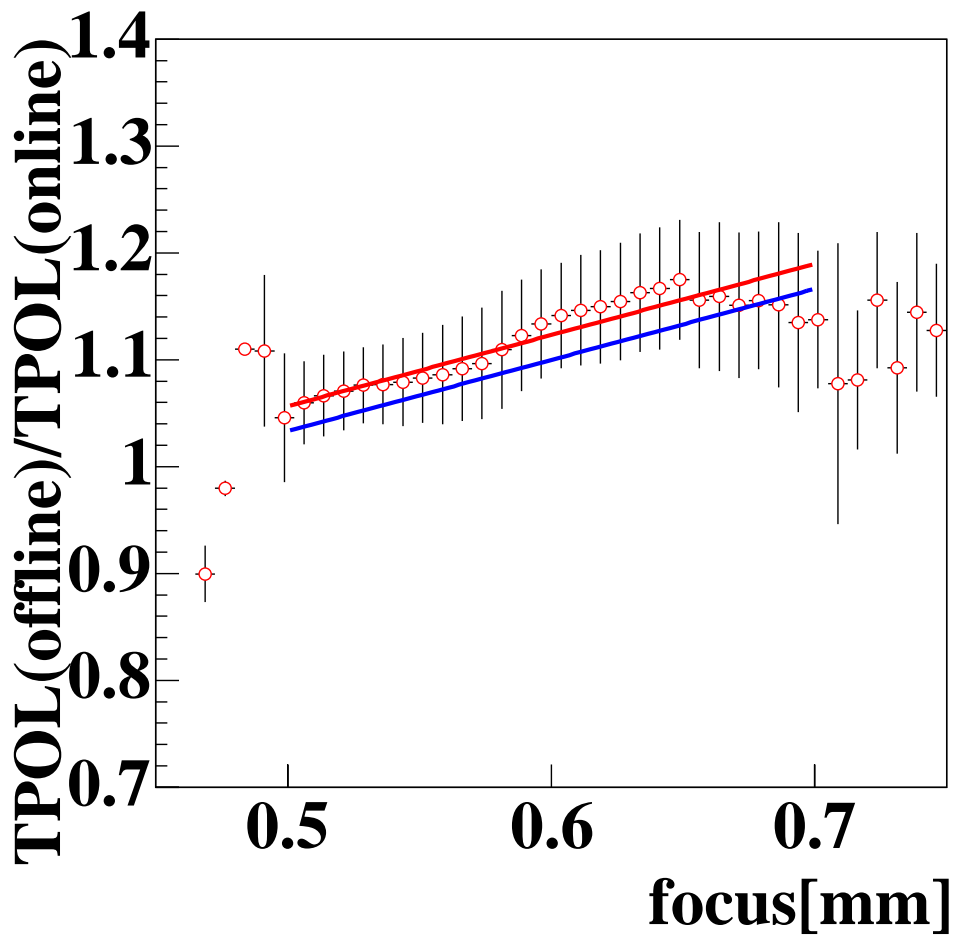


Figure 6.7: Comparison MC with the fitting method about the focus correction function. Blue line is estimated with MC and red circles and its bars are results from the fitting method. The red line is linear fit to the fitting results. On the vertical axis, offline means the fitting method and online means the averaging method.

condition can be changeable, it is natural that there is time dependence of δ_y . In the results with the averaging method, it is clearly seen the dependence to the offset and the LPOL/TPOL ratio is off from 1 as a results. The fitting method, however, can absorb the dependence and the ratio becomes almost 1. Therefore, together with the results in the previous section, it can be concluded that we can analyse the polarisation without considering the beam conditions which can be changeable at any time.

6.4 Comparison between two Polarisations \sim laser-left and laser-right \sim

Polarisation can be calculated by fit to the data stored with laser-left and laser-right separately in the fitting method. Ideally, it is expected that the two results should agree with each other if the fitting method works fine. Figure 6.10 shows the day by day difference of the two results. The polarisation calculated from laser-left is symbolised to LEFT and the one from laser-right is symbolised to RIGHT in these plots. There is apparently time dependence of the difference between the two results, besides the LEFT is always higher than the RIGHT.

Looking at the LEFT/RIGHT ratios shown in Figure 6.11, there seems to exist some systematic uncertainties since strange tails and dips emerge on the histograms with more averaging time. To see if the effects of the LEFT/RIGHT ratio propagate to the LPOL/TPOL ratio, a correlation between the LPOL/TPOL ratio and the LEFT/RIGHT ratio was checked. Judging from Figure 6.12, no strong correlation seems to be remained. Therefore, the discrepancy between the LEFT and the RIGHT does not seem to critical influence on the LPOL/TPOL ratio.

However, to investigate further about these strange structure in the ratio of the LEFT and the RIGHT, we paid attention to the η response of the calorimeter. Usually, it is expected that the η response of the calorimeter should not depend on the helicity of the laser light. Actually, looking at Figure 6.13, histograms from the fitting method seems to have some asymmetric in η between laser-left and laser-right thus the fitting method does not seem to reproduce the data exactly as for this asymmetric part. For further study, we introduced one new parameter, called “skew-factor”. The

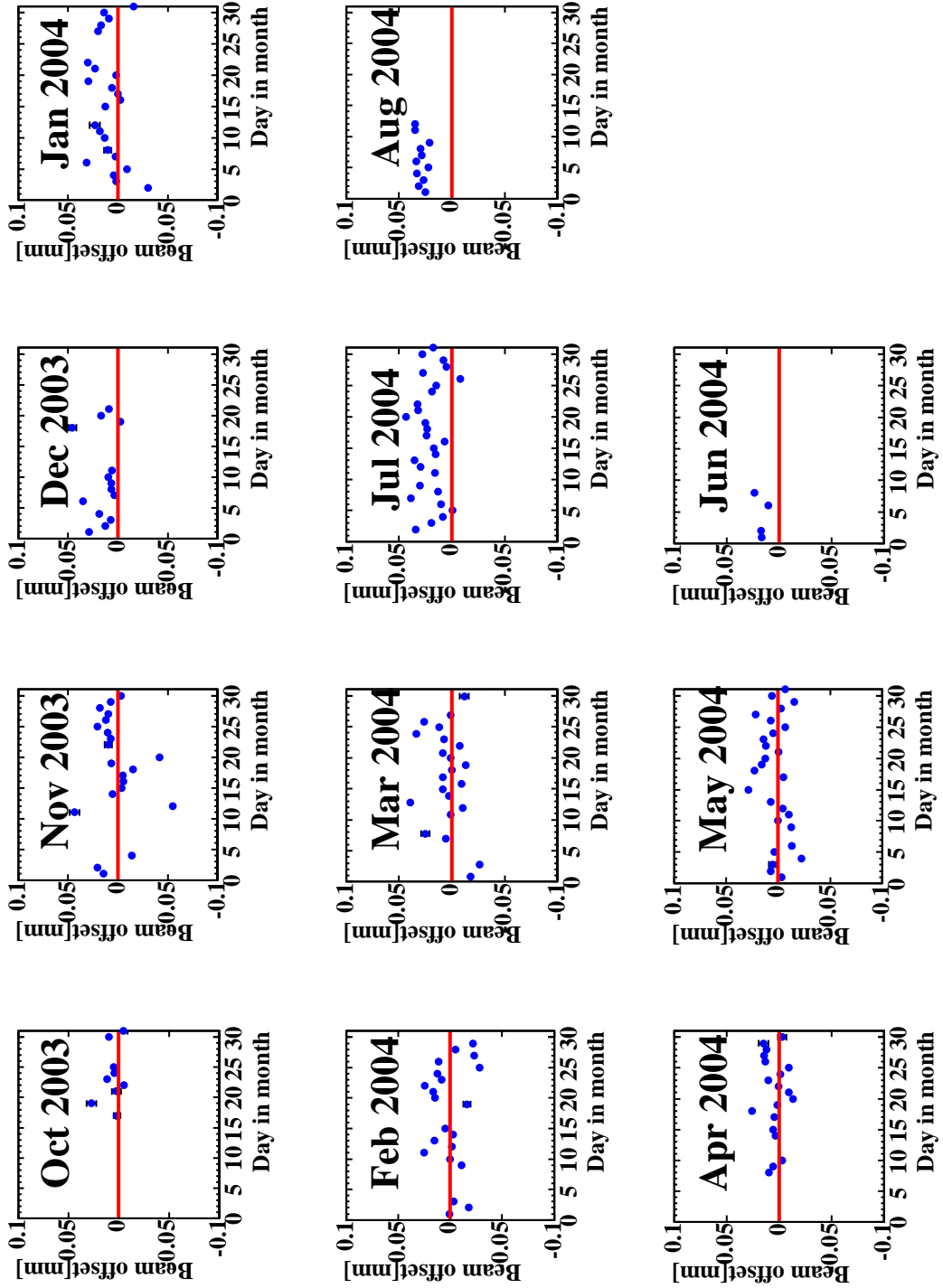


Figure 6.8: Day by day plot of δ_y . Left and middle 8 plots are from right-handed positron and right 4 plots are from left-handed positron.

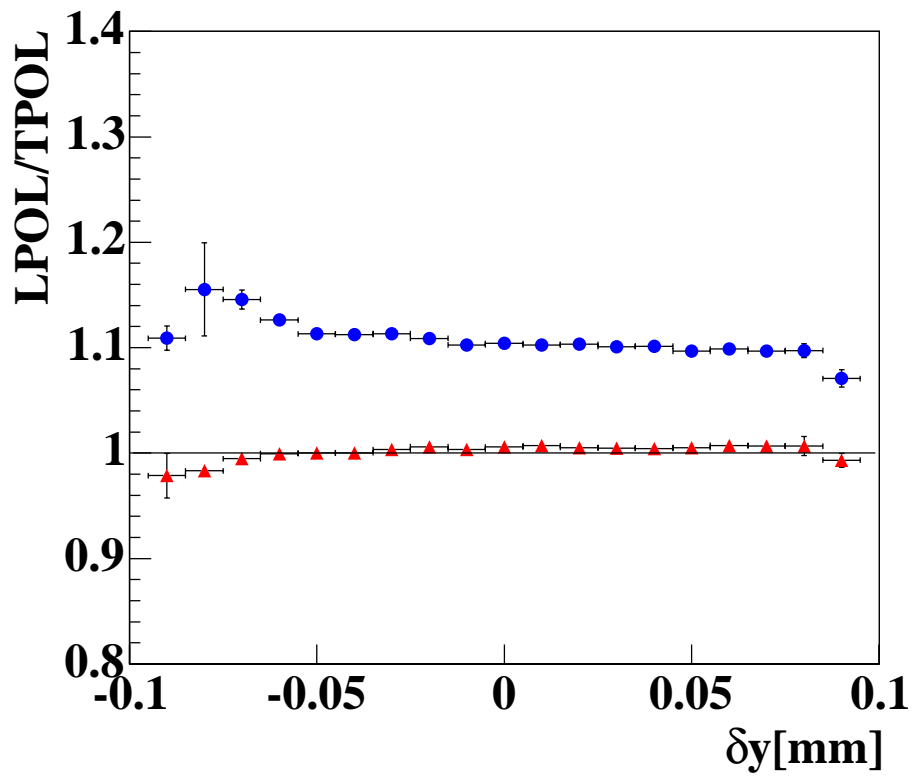


Figure 6.9: The dependence of the LPOL/TPOL ratio against δ_y . Blue dots and bars are results from the averaging method. Red ones are from the fitting method.

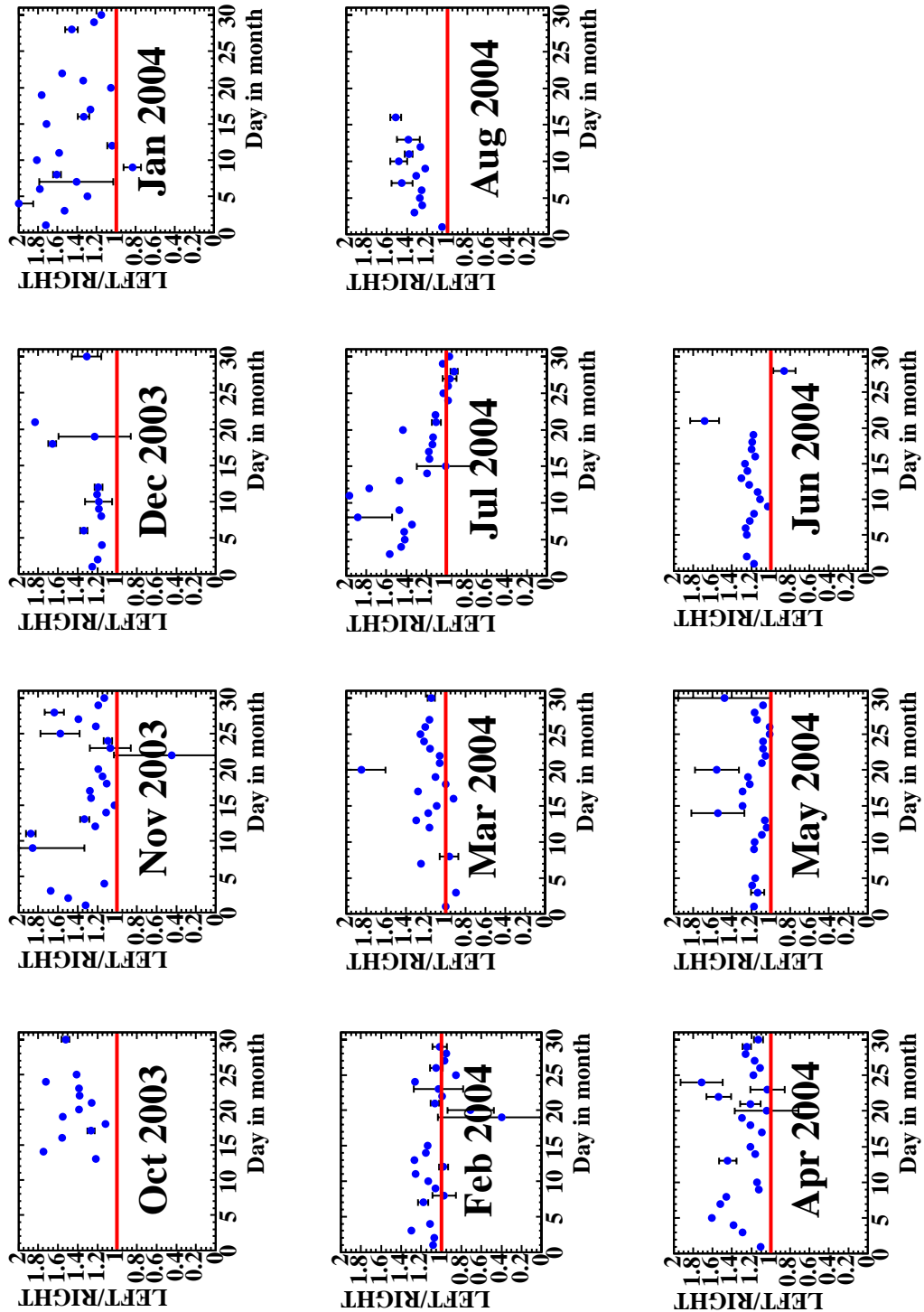


Figure 6.10: The day by day ratio plot of the polarisation from laser-left and laser-right from October 2003 to August 2004. Left and middle 8 plots are from right-handed positron beam and right 4 plots are from left-handed positron beam.

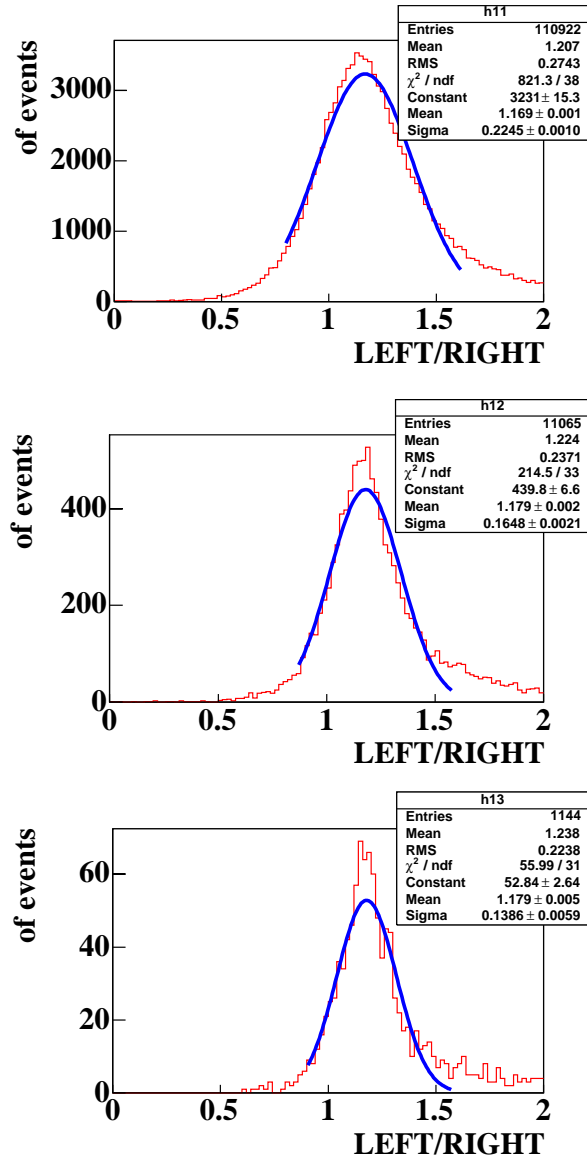


Figure 6.11: The LEFT/RIGHT ratio. From upper to lower, averaging time is increasing 1 minute, 10 minutes and 100 minutes average.

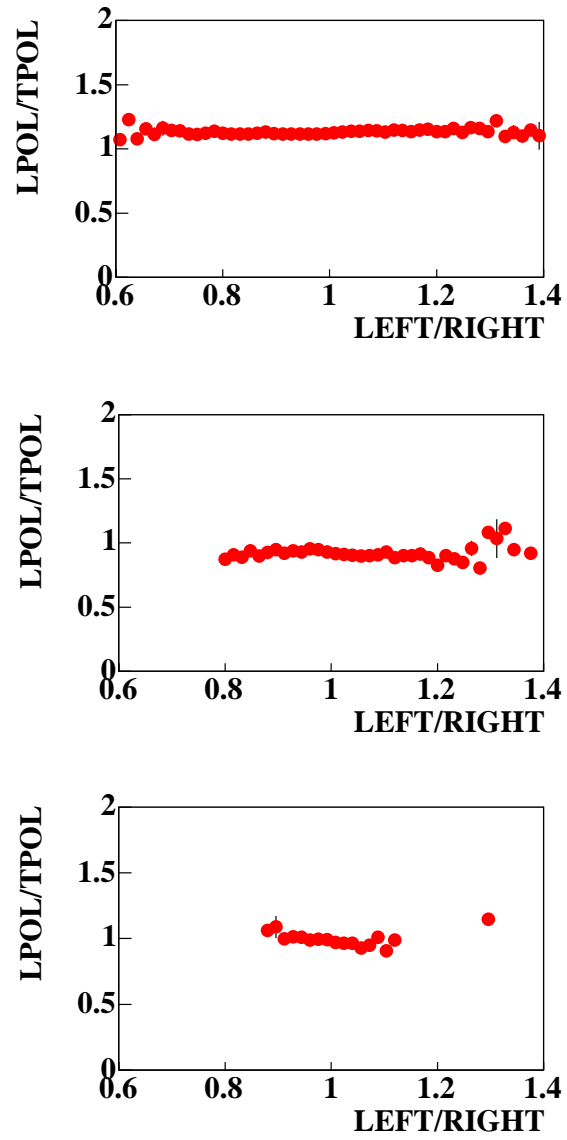


Figure 6.12: Correlation between the ratio LPOL/TPOL and the ratio LEFT/RIGHT. From upper to lower, the averaging time is 1 minute, 10 minutes and 100 minutes.

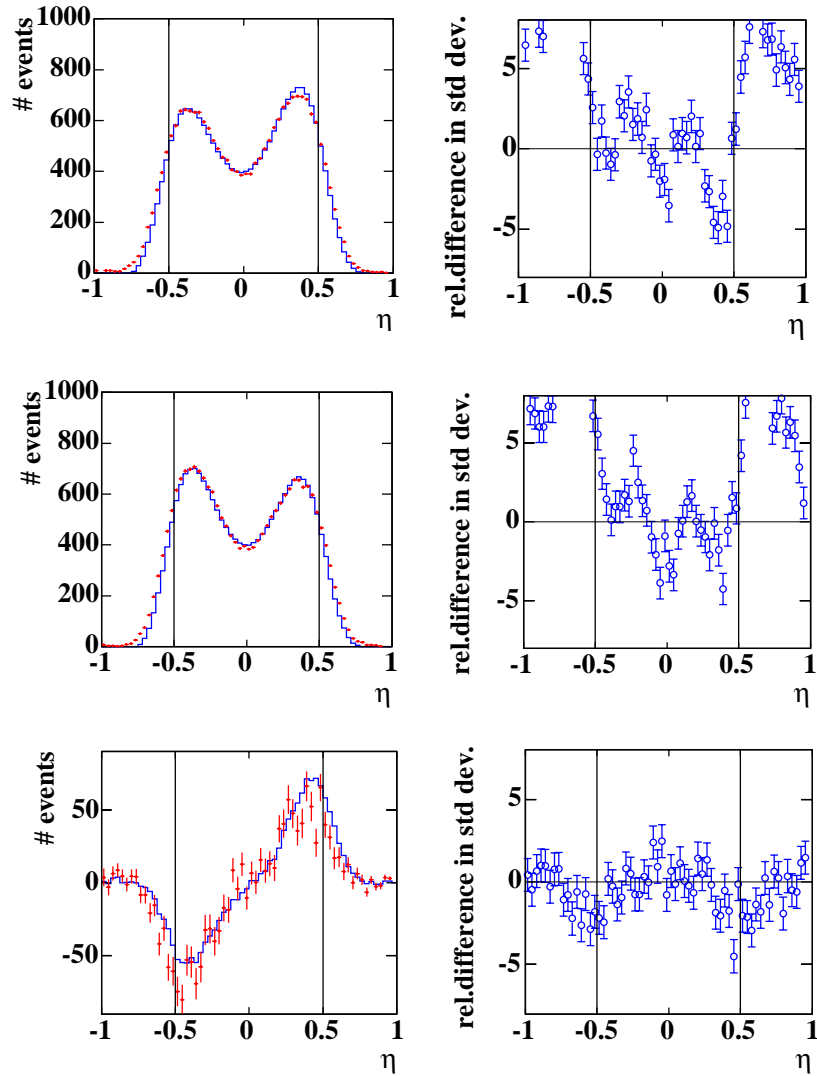


Figure 6.13: Histograms and the binwise pulls from the data and the fitting method. Left column shows histograms with laser-left, laser-right and the one subtracting laser-right from laser-left showing from upper to lower, respectively. Red dots and error bars indicate the data, the blue histogram is the end of the fitting and black lines indicate the fitting range. Right column shows the binwise pulls corresponding to each plot located the left side. The energy range is between $5.2 \text{ GeV} < E_\gamma < 11.4 \text{ GeV}$. This range is same as the averaging method and is most sensitive to the polarisation.

skew-factor “ f_{skew} ” is parameterised as:

$$\sigma_{\eta}(\eta_{true}, E_{true}) = a \sqrt{\frac{1 - \eta_{true}^2}{E_{true}}} \left(1 \pm f_{skew} \sqrt{\sqrt{|\eta_{true}|} E_{true}} \right), \quad (6.4)$$

where a is the stochastic term of the energy resolution, η_{true} and E_{true} mean same as described in chapter 4.1.

Since this parameter is made for reflecting the asymmetric η distribution, it is expected that the binwise pulls can be improved than before. In Figure 6.14, the results with the skew-factor are shown.

Then, the LPOL/TPOL ratio with the skew-factor was compared with the one without the skew-factor in more averaging time. The histograms are displayed in Figure 6.15. Looking at these histograms, strange dips are seen in the ones with the skew-factor.

Next, the LEFT/RIGHT ratio (See Figure 6.16) and the day by day difference between the LEFT and the RIGHT (See Figure 6.17) were checked again. Also, the χ^2/ndf is shown in Figure 6.18. Judging from these figures, it can be concluded as follows:

- Comparing with Figure 6.13, the binwise pulls from laser-right is actually improved and it indicates that the asymmetric distribution in η is weaker than the one without the skew-factor. (See Figure 6.14)
- The LPOL/TPOL ratios with more averaging time include extra unknown systematic uncertainty. (See Figure 6.15)
- The LEFT/RIGHT ratios are improved and are closer to 1 than the one without the skew-factor. (See Figure 6.16)
- The difference between the LEFT and the RIGHT are still observed and time dependence still remained even with the skew-factor. (See Figure 6.17)
- Actually, the mean of the χ^2 become close to 1, but strange shapes are included in the histograms with more averaging time. It means that the modelling is wrong. (See Figure 6.18)

Since strange systematic uncertainties seem to be included and the modelling for the calorimeter with the skew-factor is wrong, we conclude that the skew-factor is not necessary for the polarisation analysis. Therefore, we do not need to consider the systematic error from the skew-factor.

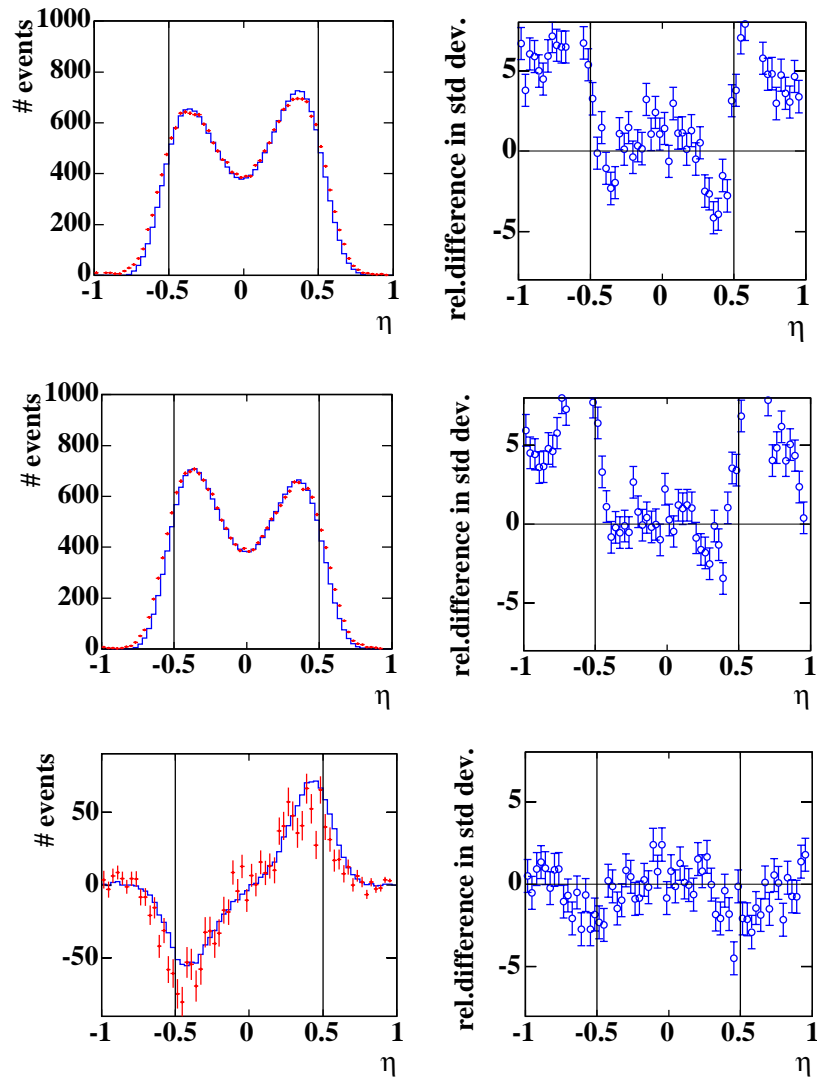


Figure 6.14: Histograms and pulls. These plots are same as Figure 6.13 except for introducing the skew-factor.

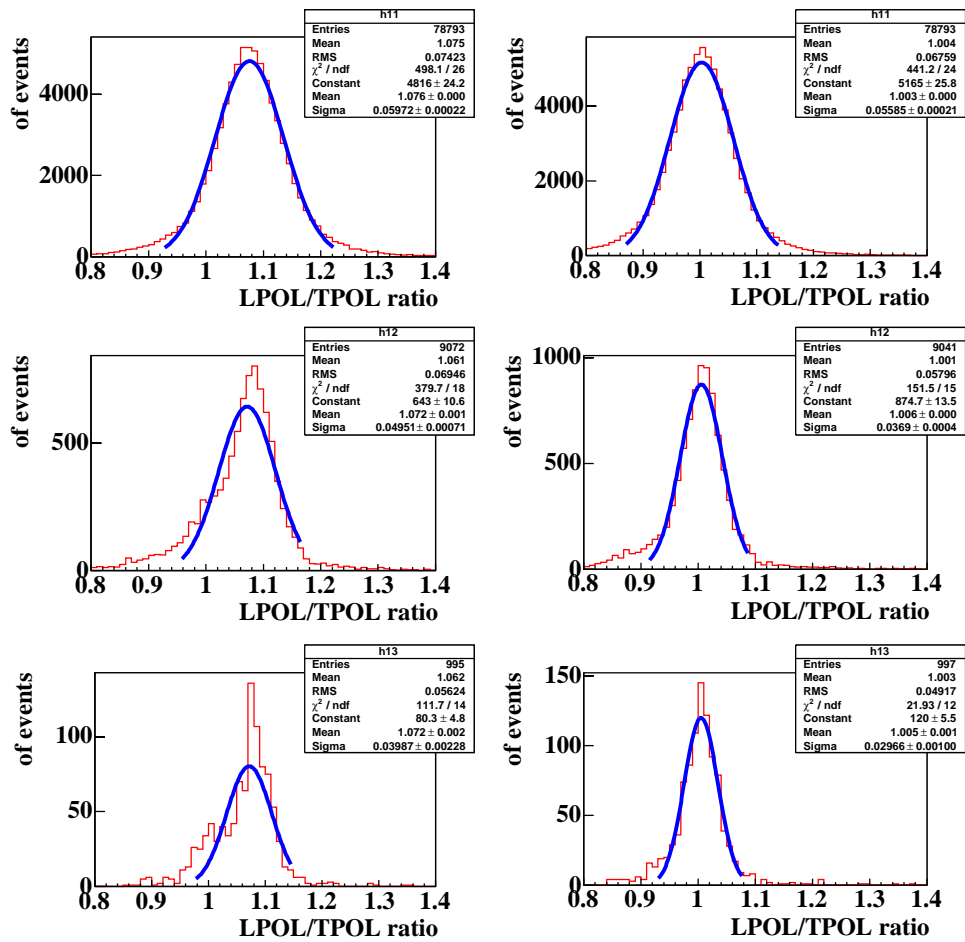


Figure 6.15: The LPOL/TPOL ratio with and without the skew-factor in more averaging time. Left columns denote the ratio with the skew-factor and right columns are without the skew-factor. Upper plots are results with 1 minute average, middles are 10 minutes average and lowers are 100 minutes average.

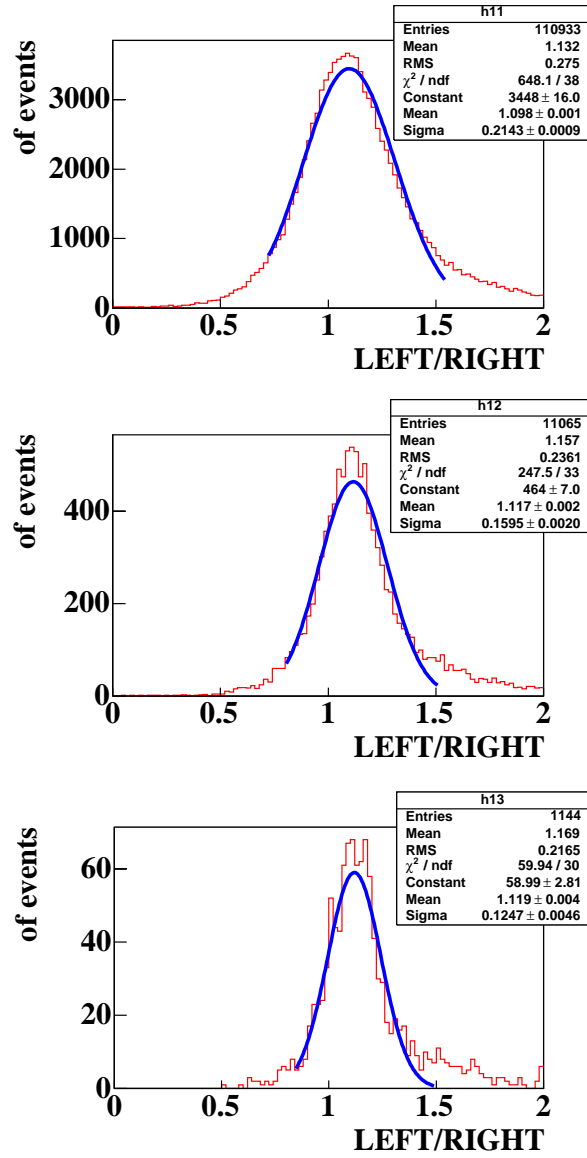


Figure 6.16: The LEFT/RIGHT ratio with the skew-factor. From upper to lower, the averaging time is 1 minute, 10 minutes and 100 minutes.

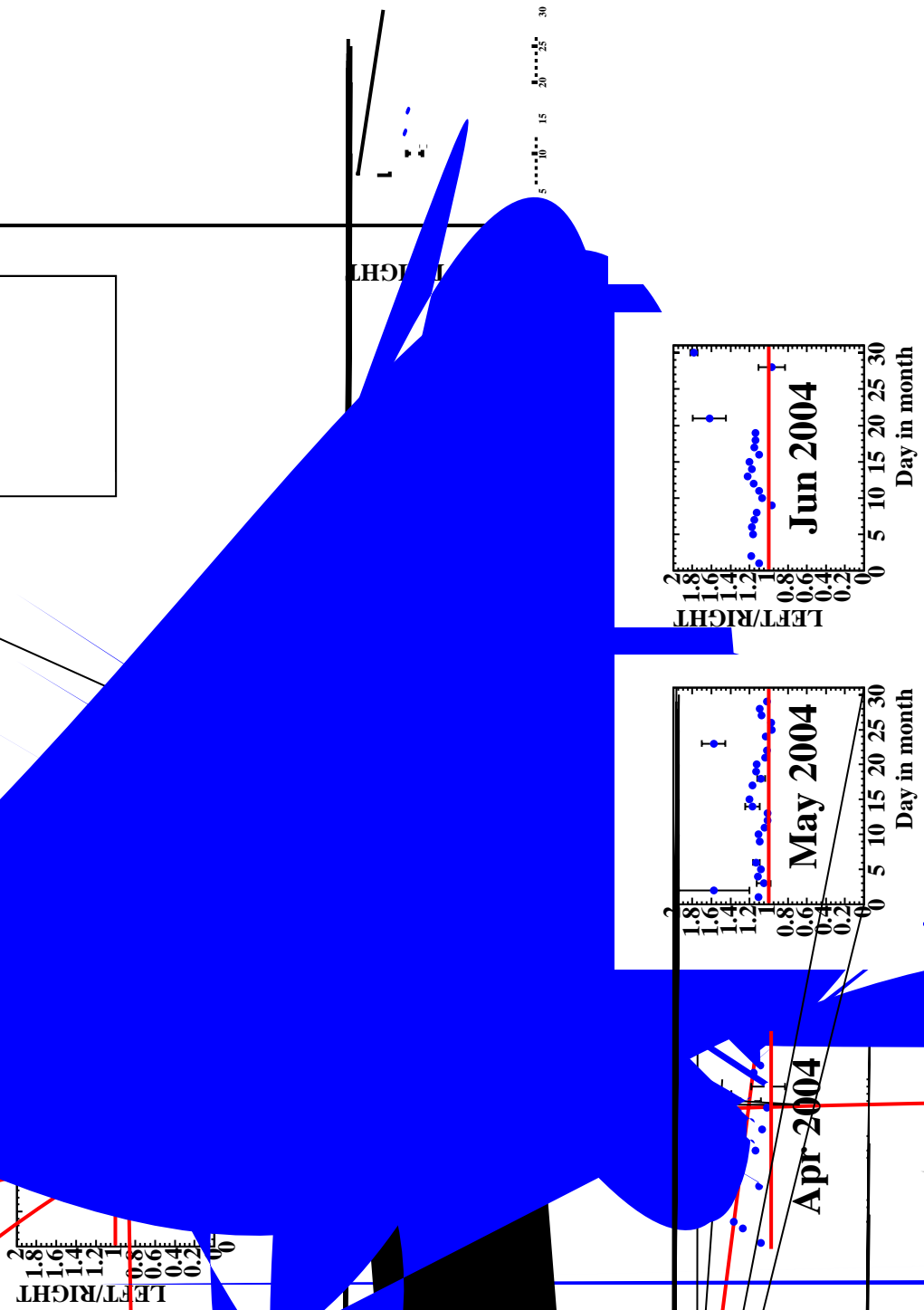


Figure 6.17: The day by day ratio of laser-left to laser-right with the skew-factor from laser-right to August 2004. Left and middle 8 plots are from right-handed positron beam and right 4 plots are from left-handed positron beam.

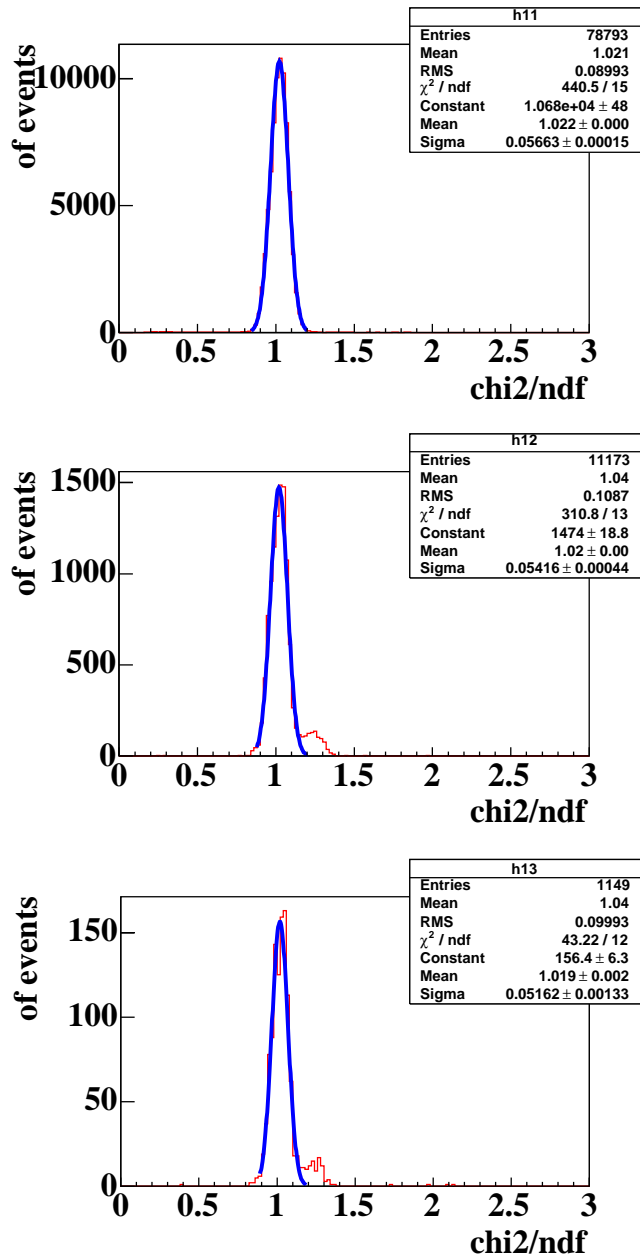


Figure 6.18: The χ^2/ndf with the skew-factor. From top to down, the averaging time is 1 minute, 10 minutes and 100 minutes.

6.5 The energy resolution

As described in the previous chapter, we needed to fix the stochastic term a to the CERN test beam value in the fitting method. However, the constant term b was free in the fitting. The reason is that the constant term does not come from the situations related to the energy, but related to the noise, the material uniformity, the light leak and so on. These things seem to depend on the experimental environment, so that we can not fix the parameter. Thus, we checked the behaviour of this parameter. Figure 6.19 shows the time dependence of the parameter. Also, the dependence of the constant term to the LPOL/TPOL ratio are shown in Figure 6.20.

Looking at the Figure 6.19, though there is slightly the time dependence of the constant term, it can be almost stable in time. If the parameter related to the detector fluctuates, the fitting can not be reliable. Also, it is seen that there is no dependence of the constant term to the LPOL/TPOL ratio. Thus these facts tell us the fitting method works fine.

6.6 The calibration of the calorimeter

Same as the constant term, parameters related to the calibration of the calorimeter, f_e and f_η , were free in the fitting since the calibration has done event by event by adjusting the high voltage of the PMTs described in the section 2.2. Thus we also have to check the behaviour of these parameters in the fitting. Figure 6.21 and Figure 6.22 show the time dependence of the parameter f_e and f_η . Also, the dependence of f_e and f_η to the LPOL/TPOL ratio are shown in Figure 6.23 and Figure . Looking at these figures, there actually exists slightly time dependence. Considering, however, the polarisation value calculated with the fitting method, we can conclude that the time dependence of the two parameters does not influence to the polarisation and the fitting method can absorb the dependence. Thus we also conclude the fitting method works fine from the fact.

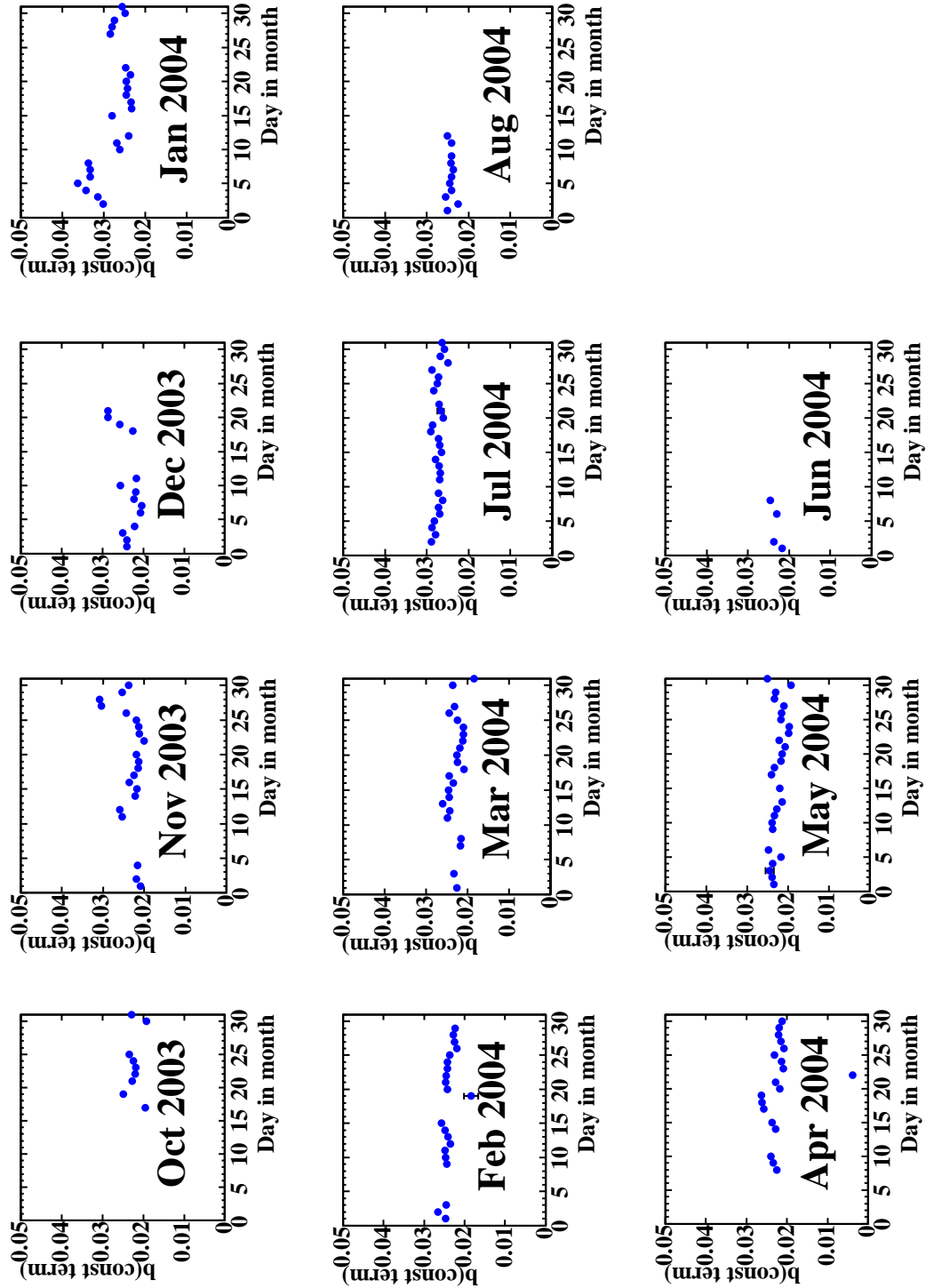


Figure 6.19: Day by day plot of the constant term. Left and middle 8 plots are from right-handed positron and right 4 plots are from left-handed positron

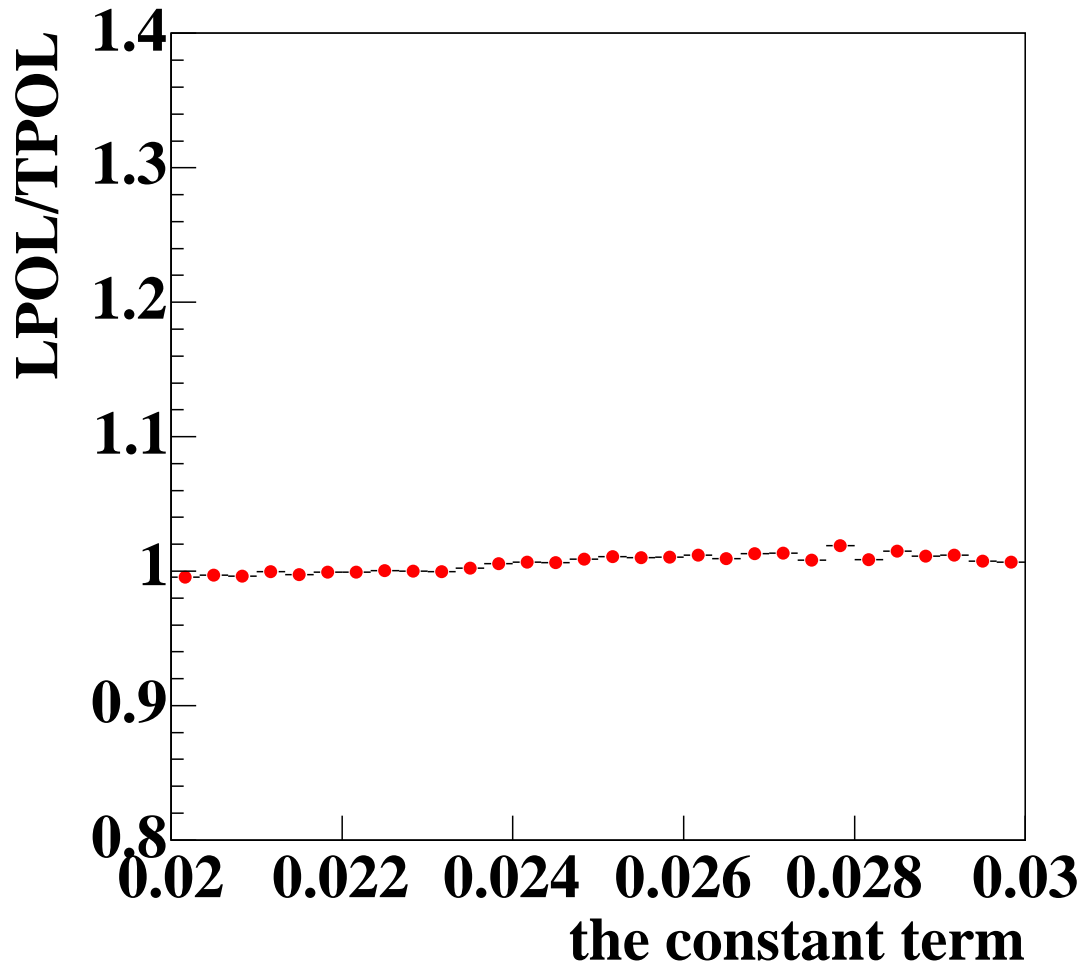


Figure 6.20: The dependence of the LPOL/TPOL ratio against the constant term.

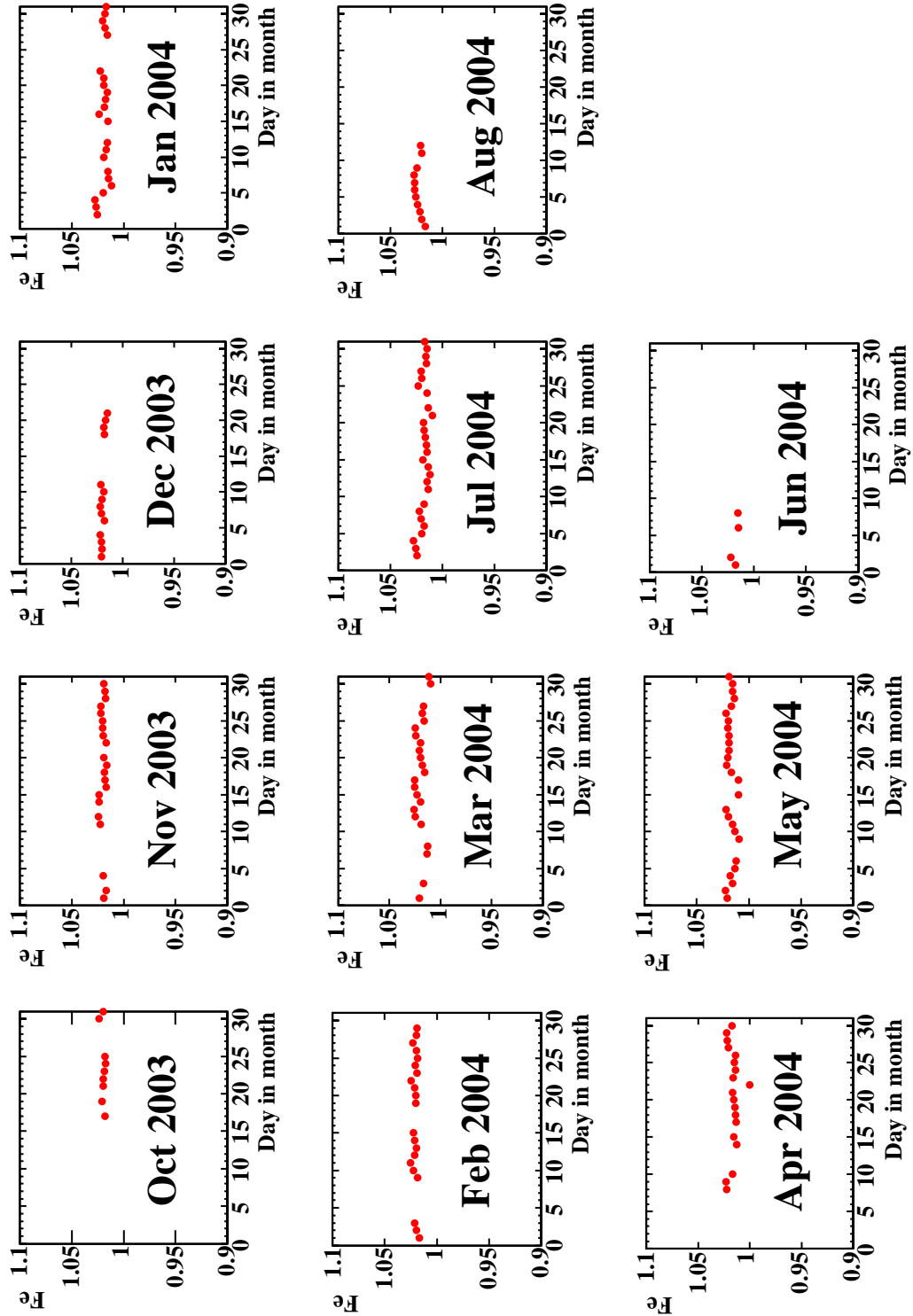


Figure 6.21: Day by day plot of parameter fe , symbolised to Fe in the plots. Left and middle 8 plots are from right-handed positron and right 4 plots are from left-handed positron

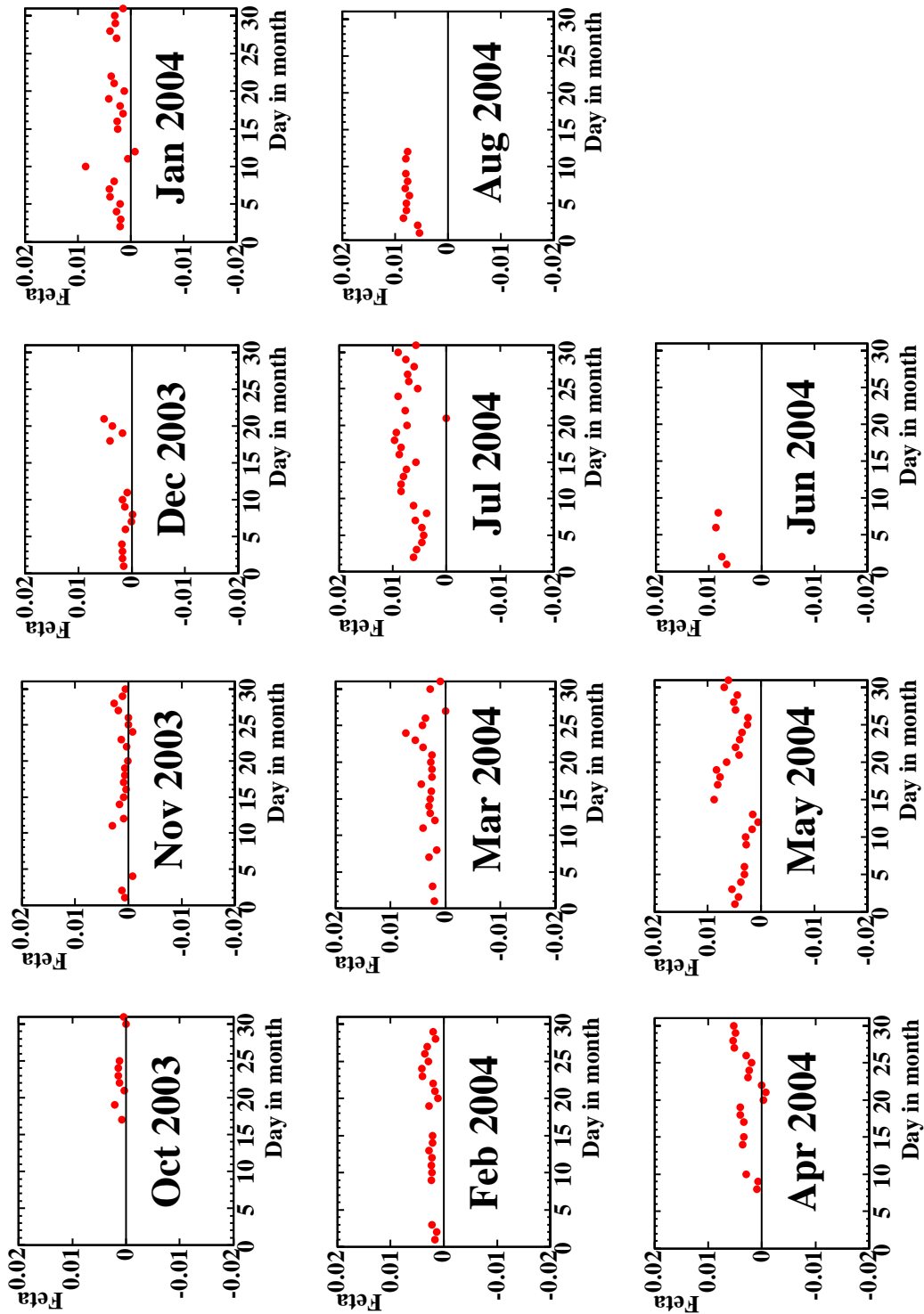


Figure 6.22: Day by day plot of parameter f_{η} , symbolised to Feta in the plots. Left and middle 8 plots are from right-handed positron and right 4 plots are from left-handed positron

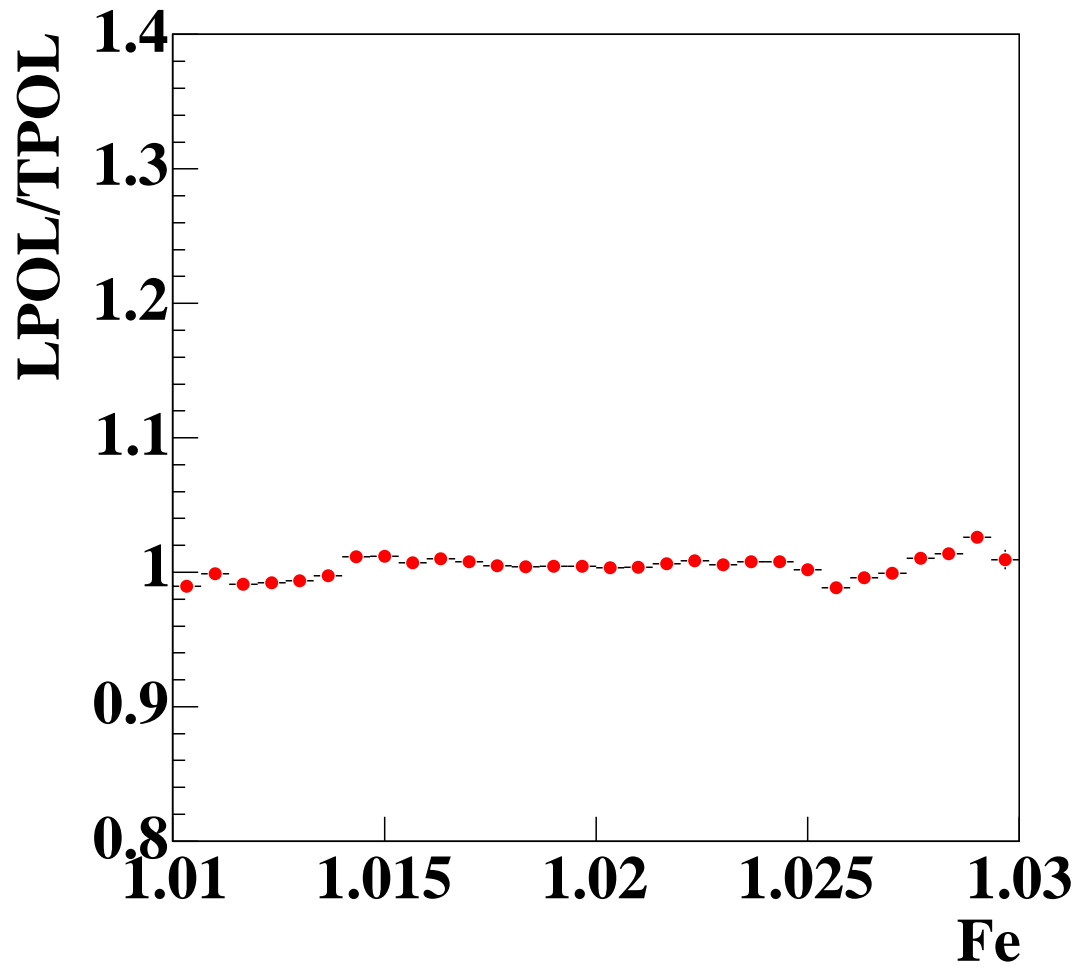


Figure 6.23: The dependence of the LPOL/TPOL ratio against f_e , symbolised to Fe in the plot.

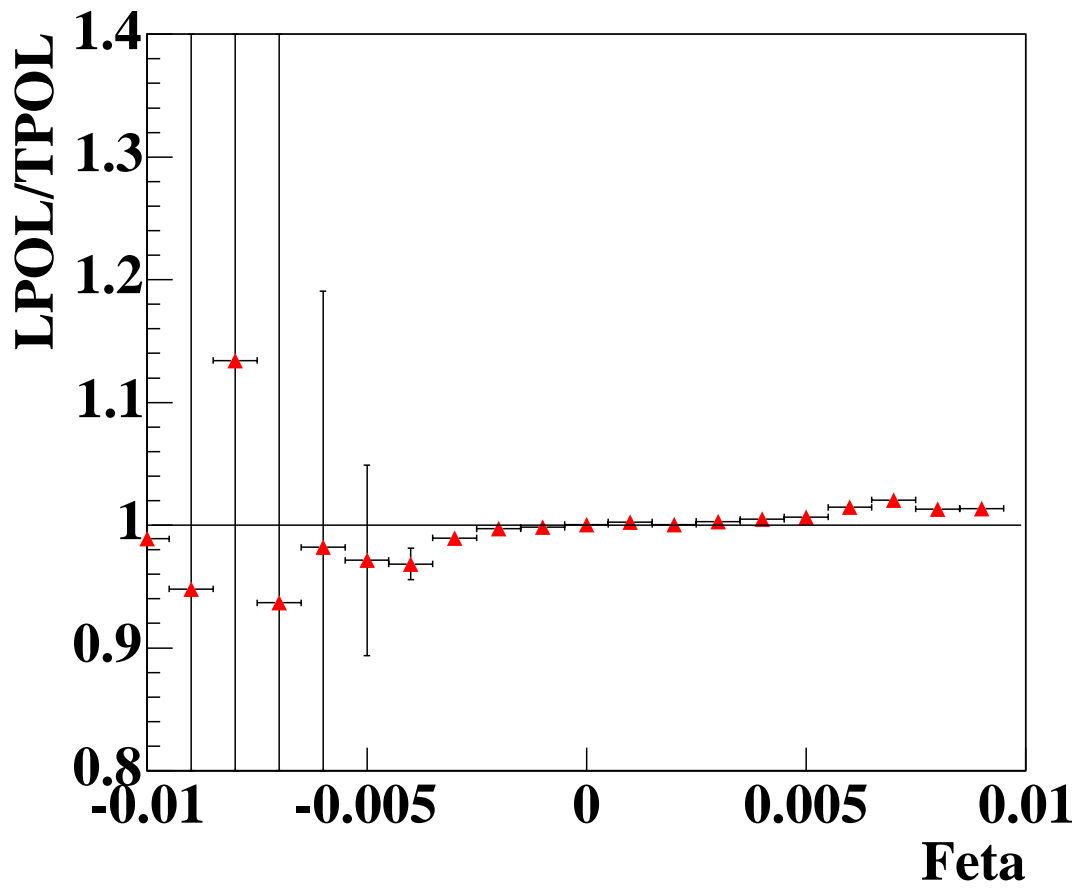


Figure 6.24: The dependence of the LPOL/TPOL ratio against f_η , symbolised to Feta in the plot.

Chapter 7

Conclusion

The polarisation of lepton beam has been measured at HERA. The ratio of LPOL and TPOL has been off 10% from 1 and this puzzle has made people embarrassed for a long time. The averaging method which has been used for polarisation measurement depends on the beam condition, so that this method is not suitable in the situation where conditions related beam can be changeable. To eliminate these disadvantages, a new analysis method has been developed, called “the fitting method”. In this paper, some results using the fitting method has been reported.

We have analysed all data from October 2003 to August 2004 with the fitting method. The fitting method works fine and the LPOL/TPOL ratio calculated with the fitting method become close to 1, these two values agree with each other within 1%. Also, the ratio does not seem to have strange dips and the σ of the histograms is getting smaller with more averaging time. It indicates that polarisation can be calculated without critical systematic uncertainty with the fitting method.

We have checked the dependence of beam to the polarisation measurement. In averaging method, there are clearly dependence of the focus size, which causes critical error to the measurement, and the dependence of δ_y . From the analysis with the fitting method, the focus size dependence and the δ_y dependence are hardly seen and also the fitting method could reproduce the focus correction function which was estimated by MC.

We have evaluated systematic errors from various sources. As a results, it is

concluded that total systematic error is controlled within 3%. This is mainly due to the imperfectness of the calibration of the calorimeter and the fitting range in η . At present, we have not study fully at these points thus these errors are estimated by educational guess. With more study, errors from these sources can be smaller.

There seemed to have η asymmetric distributions in the binwise pulls for both laser-left and laser-right. To study this asymmetry further, we introduced one new parameter, “the skew-factor”, to reflect the asymmetry. Due to the asymmetries in the binwise pulls, there was apparently time dependence of the difference between the LEFT and the RIGHT. Besides, the LEFT/RIGHT ratio was off from 1 by 10%. Though the binwise pulls was improved with the skew-factor, the LEFT/RIGHT ratios and the time dependence were not improved drastically. Besides, the LPOL/TPOL ratio was off from 1 by 7% and included some unknown systematic uncertainties with more averaging time. This fact indicates that the modelling with the skew-factor for the calorimeter was wrong thus we do not need to the skew-factor and should not consider the 7% error as a total systematic error.

In the fitting method, we considered some parameters, b , σ_y , δ_y , f_e and f_η as a free parameter. As a fitting results, these parameters have no critical dependence to the LPOL/TPOL ratios although there are slightly time dependence. Therefore, it can be concluded that the fitting method is suitable for the polarisation analysis and works fine.

Acknowledgements

I really appreciate Prof. R. Hamatsu for his guidance, support and giving me to join the ZEUS collaboration and to study this analysis. I express thanks to Prof. K. Tokushuku for his guidance, support and valuable advices for my study.

I really special many thanks to Dr. K. Nagano. He always support me and has many discussions with me for this analysis. Also, I appreciate for reading and commenting on this manuscript. Without his help and his comment, I most probably could not continue this study. They were vital for this analysis.

I am deeply grateful to Dr. Y. Yamazaki. His comments and advices were great helpful for me. I also express great thanks to Dr. K. Matsuzawa, Dr. S. Schmitt, Prof. V. Gharibyan. They gave me many suggestions and proposals on the meeting, especially the discussion with Dr. S. Schmitt were most important for my analysis.

I sincerely thank Prof. F. Corriveau, Prof. T. Behnke, Dr. S. Schmitt for their guidance and organisation of the polarimeter meeting and I appreciate all members of POL2000 Group.

I thank members of the ZEUS-Tokyo group, Prof. S. Yamada, Prof. M. Kuze, Prof. T. Tsurugai, Prof. S. Kitamura, Prof. Y. Iga. They gave me helpful advices on the monthly meeting.

I express thanks to Prof. T. Sumiyoshi, Prof. C. Fukunaga for their careful comments for this thesis. I am thankful to Dr. M. Chiba, Dr. T. Kumita for giving special advice for my study.

I also many thanks to Dr. T. Kohno, Mr. S. Kagawa, Mr. T. Tawara, Ms. M. Kataoka, Mr. H. Kaji, Mr. Y. Ri, Ms. S. Kato, Mr. H. Fujimoto, Mr. R. Hori, Ms. S. Shimizu, Mr. K. Tsurusaki, Mr. H. Furuta, Mr. J. Maeda and Mr. T. Takai for many joyful communications and spending happy time in Germany.

I thanks to all members of high energy group in TMU, especially Mr. A. Ishimizu, Mr. H. Fujimoto and Mr. S. Yamamoto for having good time and talking a lot.

Finally, I really appreciate for my family. They always support me and keep their eyes on me in my life. and...special many many thanks to Anna;))

Bibliography

- [1] F. Halzen and A.D. Martin, *Quarks and Leptons: An Introductory Course in Modern Particle Physics*, John Wiley Sons, 1984.

- [2] S.L. Glashow, *Nucl. Phys.* **22**(1961) 579;
S. Weinberg, *Phys. Rev. Lett.* **19**(1967) 1264.

- [3] The ZEUS detector. Status Report (unpublished), DESY, 1993.

- [4] R.Hamatsu, Study of radiation dose in the silicon detector of the Transverse Polarimeter using GEANT. 2000.

- [5] S.Kato, A study of the silicon detector of the TPOL at HERA, for TMU master thesis. 2004.

- [6] A.A.Sokolov, I.M.Ternov, V.V.Mikhailin, *Izv. Vuz. Fiz.* 4(1976) 7.

- [7] M.Ruth et al., Construction and Beam Test of a Spare Calorimeter for the HERA Transverse Polarimeter. Internal Polarimeter Report 97-05 (1997).

- [8] S.Schmitt, presented at the Polarimeter meeting, 8th June, 2004.

- [9] D.P.Barber et al., *Nucl. Inst. Meth.* **A329**, 79 (1993).

- [10] T.Behnke et al..The Transverse Polarimeter (TPOL) Test Beam at CERN in July-August 2001. October 2002, ZEUS-02-019.

- [11] V.Gharibyan, in private communication.

- [12] C.Fry, in private communication.

- [13] F.Corriveau, V.Gharibyan, O.Ota, S.Schmitt and the POL2000 group. A Calibration of the HERA Transverse Polarimeter for the 2003/2004 Data (unpublished). July 2004.